学位論文

Stratospheric HCl, HF, and N_2O in Antarctica observed with solar infrared absorption method

赤外吸光分光観測に基づく南極成層圏 HCl, HF, N_2O の研究

平成 5 年 12 月 博士 (理学) 申請

東京大学大学院理学系研究科
地球惑星物理学専攻
村　田　　功

①

学位論文

Stratospheric HCl, HF, and N_2O in Antarctica observed with solar infrared absorption method

赤外吸光分光観測に基づく南極成層圏 HCl, HF, N_2O の研究

平成 5 年 12 月 博士 (理学) 申請

東京大学大学院理学系研究科
地球惑星物理学専攻
村　田　　功

Abstract

Vertical column densities of HCl, HF, and N_2O were observed using solar infrared absorption technique at Syowa Station (69.006° S, 39.590° E), to study the chemistry and dynamics of Antarctic ozone depletion.

The solar spectra were taken by using a 1.5m double-pass grating monochromator with wavenumber resolution of 0.075cm^{-1} - 0.137cm^{-1}, and the measurements were carried out from July to December 1991.

HCl vertical column densities were observed to be (1.65±0.43) × 10^{15}cm^{-2} in winter and to increase to (6.07±1.20) × 10^{15}cm^{-2} in summer. HF and N_2O vertical column densities remained fairly constant at (1.31±0.25) × 10^{15}cm^{-2} and (5.98±0.31) × 10^{18}cm^{-2}, respectively from July to December, suggesting stable dynamical conditions. The temporal variation of the HF/HCl vertical column density ratios shows that only HCl was removed by chemical reactions during polar night. These reactions might occur on the surfaces of the polar stratospheric cloud (PSC) particles in the altitude region between 12km and 25km. The decrease in HCl vertical column density ((4.4±1.6) × 10^{15}cm^{-2}) during polar night implies that almost all HCl molecules in this altitude region were converted into other chlorine species and/or trapped in the PSC particles.

Total ozone measured with a Dobson spectrophotometer shows that Syowa Station was located in the 'ozone hole' in mid-November, whereas the HCl vertical column density had recovered to the summer level at that time. Atmospheric temperature and wind measured with radiosondes over Syowa Station exhibit that the air mass in the 'ozone hole' remained dynamically stable in August and September. The increase in HCl vertical

column density from September to November is thought to be mainly due to chemical reactions. Comparing the observational result with a one-dimensional time-dependent photochemical model calculation, it is found that a half of the decreased amount of HCl vertical column density was converted into active chlorine and that the remainder was converted into other less active chlorine species and/or trapped in the PSC particles.

Contents

1 Introduction

In this study vertical column densities of HCl, HF, and N_2O were observed using solar infrared absorption technique at Syowa Station, Antarctica.

Hydrogen chloride (HCl) is a relatively chemically stable molecule in the stratosphere. It is supposed to be a reservoir for stratospheric chlorine species. Stratospheric chlorine plays an important role in the ozone destruction processes, particularly in the Antarctic ozone depletion. The behavior of HCl is crucial to understand the chemistry of the Antarctic ozone depletion.

Hydrogen fluoride (HF) is a chemically stable molecule in the stratosphere and HF as well as HCl are produced from chlorofluorocarbons (CFCs). Observations of both HCl and HF in the stratosphere provide information on the chemical activity of HCl.

Nitrous oxide (N_2O) also is a stable molecule in the lower stratosphere. Therefore, both HF and N_2O are supposed to be tracers of the atmospheric motion.

1.1 Stratospheric hydrogen chloride

1.1.1 Overview of stratospheric chlorine chemistry

Some atmospheric chlorine species are produced at the earth's surface through both natural and anthropogenic processes. For example, methyl chloride (CH_3Cl) is believed to be produced mainly from the oceans and by biomass burning in particular by tropical agricultural practices. Carbon tetrachloride (CCl_4) is produced as an intermediate during industrial chemical manufacturing. CFCs such as $CFCl_3$ (CFC-11), CF_2Cl_2 (CFC-12), and $C_2F_3Cl_3$ (CFC-113) are produced in large quantity for use as refrigerants, foam

blowing agents, solvents, and aerosol propellants. The 1992 global mean tropospheric concentrations were 600 pptv for CH_3Cl, 132 pptv for CCl_4, 268 pptv for CFC-11, 503 pptv for CFC-12, and 82 pptv for CFC-113 [WMO, 1994]. The anthropogenic chlorine species contribute about 80 % of the total chlorine. Though the production of these anthropogenic chlorine species is going to be restricted by the Montreal Protocol, there already exist a large amount of anthropogenic chlorine species in the atmosphere and they are producing reactive chlorine species.

These chlorine containing species are quite stable in the troposphere, but when they are transported to the stratosphere, they produce chlorine atom and chlorine monoxide (ClO) through photodissociation and the subsequent reactions. For example,

$$CFCl_3 + h\nu \longrightarrow CFCl_2 + Cl \qquad \text{(R1)}$$
$$CFCl_2 + O_2 \longrightarrow COFCl + ClO, \qquad \text{(R2)}$$

COFCl is photodissociated, further to release chlorine (or fluorine) atoms. Cl and ClO are very active and provide an important catalytic cycle which destroys odd oxygen.

$$\begin{array}{lllllll} & Cl & + & O_3 & \longrightarrow & ClO & + & O_2 & \text{(R3)} \\ & ClO & + & O & \longrightarrow & Cl & + & O_2 & \text{(R4)} \\ \hline \text{net:} & O_3 & + & O & \longrightarrow & & & 2\,O_2. & \text{(R5)} \end{array}$$

This catalytic cycle is effective in the upper stratosphere (around 40 km in altitude). In the lower stratosphere, it can't work effectively because of low concentration of atomic oxygen. ClO also react with nitric oxide (NO),

$$ClO + NO \longrightarrow Cl + NO_2, \qquad \text{(R6)}$$

and with nitrogen dioxide (NO_2),

$$ClO + NO_2 + M \longrightarrow ClONO_2 + M \qquad \text{(R7)}$$

where M is the third body of the reaction (N_2 or O_2). $ClONO_2$ is a reservoir of chlorine and nitrogen species. Reactions (R6) and (R7) represent important couplings between the chlorine and nitrogen cycles. In addition to rapid processes (R3), (R4), (R6), and (R7), there are slower processes which convert these active chlorine species into HCl that is an chlorine reservoir. Active chlorine species are removed through the following reactions:

$$Cl + CH_4 \longrightarrow HCl + CH_3 \quad \text{(R8)}$$
$$Cl + HO_2 \longrightarrow HCl + O_2 \quad \text{(R9)}$$
$$Cl + H_2 \longrightarrow HCl + H. \quad \text{(R10)}$$

(R8) is the most important and (R9) is important in the upper stratosphere.

HCl reacts with OH and O to reproduce Cl,

$$HCl + OH \longrightarrow Cl + H_2O \quad \text{(R11)}$$
$$HCl + O \longrightarrow Cl + OH. \quad \text{(R12)}$$

These processes provide the principal source of active chlorine species in the upper stratosphere. HCl and active chlorine species are balanced in the stratosphere through reactions (R8) - (R12), and thereby the depletion rate of odd oxygen is affected by the HCl amount.

1.1.2 Review of stratospheric HCl researches

The primary source of HCl in the stratosphere is the photodissociation of halocarbons as mentioned above, and minor fraction results from the reaction of OH with CH_3Cl and from the direct injection of HCl into the stratosphere due to huge volcanic eruptions. The effect of volcanic injections is largely uncertain. A relatively large increase of stratospheric HCl was observed after the eruptions of El Chichón volcano in 1982 [Mankin and Coffey, 1984], but a small or no increase was observed after the eruption of Mt. Pinatubo in 1991 [Mankin *et al.*, 1992; Wallace and Livingston, 1992]. HCl is produced through other processes in the troposphere. In the marine boundary layer, HCl is produced primarily

through the interaction of SO_4^{--} and NO_3^- ions with NaCl in ocean spray, and some HCl is produced in plastics burning and through certain industrial processes. The principal sink of HCl is rainout in the troposphere. Since HCl is highly soluble in water, it is easily removed from the atmosphere when it is transported downward into the troposphere. This is also the main sink of the chlorine species.

A vertical distribution of HCl is expected to have a minimum in the lower stratosphere and upper troposphere because HCl is mainly produced in the upper stratosphere and in the marine boundary layer. There are a limited number of observations of the vertical distributions of HCl. The result of the Balloon Intercomparison Campaigns shows that mixing ratios increase with altitude in the stratosphere [WMO, 1986; Farmer *et al.*, 1990]. The observed mixing ratios are about 0.5 ppbv at an altitude around 20 km increasing to about 2 ppbv at an altitude around 50 km.

There are some observations on the latitudinal distributions of the stratospheric column densities of HCl. Mankin and Coffey [1983] determined the vertical column densities above 12 km by measuring solar infrared absorption spectra with a Fourier transform spectrometer flown on an aircraft. They made 34 flights over a five year period from 1978 to 1982, covering the latitude range from 4.6°N to 70.8°N. They reported that the HCl column density varied from $0.7 \times 10^{15}\mathrm{cm}^{-2}$ around the equator to $2.7 \times 10^{15}\mathrm{cm}^{-2}$ at 70°N latitude with an estimated accuracy of 25 %. Girard *et al.* [1983] also used a spectrometer flown on an aircraft and determined the vertical column densities above 11.5 km. They made 9 flights in April and May of 1980, covering the latitude range from 62°N to 60°S. Their results show a minimum which is below their detection limit of $0.8 \times 10^{15}\mathrm{cm}^{-2}$ at the equator and a maximum of $3.0 \times 10^{15}\mathrm{cm}^{-2}$ at 62°N latitude with an

estimated accuracy of 25 %. Though the values of Girard are larger than those of Mankin and Coffey, the relative latitudinal distributions are quite similar with each other. This latitudinal distribution indicates that HCl are transported poleward by a global circulation and accumulate in the lower stratosphere to some extent before they enter into the troposphere.

Mankin and Coffey [1983] also reported the long-term trend of HCl. They determined an increase rate of 5 % yr^{-1} at mid-latitudes, but its uncertainty is large. Rinsland *et al.* [1991] reported an increase rate of (5.1±0.7) % yr^{-1} from the ground-based infrared spectroscopic observations at Kitt Peak (altitude 2.09 km; 31.9°N, 111.6°W) during the period between 1977 and 1990. Some other observations show an increase rate of several percent per year. Seasonal variations are reported by Rinsland *et al.* [1991]. Their results show a maximum in early spring and a minimum in early fall with a peak-to-peak amplitude of 13 % in HCl vertical column density. In addition, there is short-term variability in a time scale of a day. For example, about 30 % of variations in HCl column density were observed within a day at Jungfraujoch Station (altitude 3.58 km; 46.65°N, 8.0°E) [Zander *et al.*, 1987b]; however, a systematic diurnal variation pattern was not significant.

1.1.3 HCl in the Antarctic ozone depletion

In this study, the author observed HCl vertical column densities in Antarctica. Chlorine chemistry is supposed to play an important role in the formation of the Antarctic ozone depletion, so called 'ozone hole' discovered by Farman *et al.* [1985], and the behavior of HCl is important to understand the chemistry of the Antarctic ozone depletion.

The Antarctic ozone depletion has the following characteristics.

1. Ozone decrease begins in early spring (August or September) when the sunlight comes back to Antarctica and the depletion continues till October or November.

2. The depletion occurs mainly in the altitude region between 12 and 25 km.

3. The magnitude of the depletion becomes larger year after year.

These characteristics can't be explained in terms of stratospheric gas-phase chemistry which had been considered before the discovery of the Antarctic ozone depletion. It has been recognized through many observations and theoretical models that heterogeneous processes occurring on the surface of aerosol particles play important roles [e.g., Solomon, 1990]. The following is the outline theory which is the most reasonable at present.

During winter and early spring, an isolated polar vortex is formed in the Antarctic lower stratosphere. It is stable enough to prohibit the mixing of cold polar air with warmer mid-latitude air. This results in a strong temperature contrast between the Antarctic and the mid-latitudes of the southern hemisphere. The temperature in the Antarctic lower stratosphere become cold enough to form solid particles called polar stratospheric clouds (PSCs). PSC particles can provide the surface which catalyze heterogeneous chemical reactions. The principal reactions that have been investigated are

$$ClONO_2(g) + HCl(a) \longrightarrow Cl_2(g) + HNO_3(s) \quad (R13)$$
$$ClONO_2(g) + H_2O(a) \longrightarrow HOCl(g) + HNO_3(s) \quad (R14)$$
$$HOCl(g) + HCl(a) \longrightarrow Cl_2(g) + H_2O(s) \quad (R15)$$
$$N_2O_5(g) + HCl(a) \longrightarrow ClONO(g) + HNO_3(s) \quad (R16)$$
$$N_2O_5(g) + H_2O(a) \longrightarrow 2HNO_3(s). \quad (R17)$$

where (g) indicates gas phase, (s) indicates solid crystalline, and (a) indicates surface-adsorbed molecule. These reactions convert the reservoir species HCl and $ClONO_2$ into

the reactive species Cl_2, HOCl, and ClONO, and convert nitrogen oxides into the reservoir species nitric acid (HNO_3). When the sunshine returns to hit the Antarctic atmosphere after winter, Cl_2, HOCl, and ClONO are photodissociated to produce Cl or ClO. Ozone is destroyed through the catalytic cycle involving the ClO dimer ($(ClO)_2$).

$$
\begin{array}{lllllllllll}
2\,(& Cl & + & O_3 & & \longrightarrow & ClO & + & O_2 &) & & (R18) \\
 & ClO & + & ClO & + & M \longrightarrow & (ClO)_2 & + & M & & & (R19) \\
 & (ClO)_2 & + & h\nu & & \longrightarrow & Cl & + & ClOO & & & (R20) \\
 & ClOO & + & M & & \longrightarrow & Cl & + & O_2 & + & M & (R21) \\
\hline
\text{net:} & 2\,O_3 & + & h\nu & & \longrightarrow & & & 3\,O_2. & & & (R22)
\end{array}
$$

Another catalytic cycle involving ClO and bromine oxide (BrO) also contributes to the ozone destruction,

$$
\begin{array}{lllllllll}
 & Cl & + & O_3 & \longrightarrow & ClO & + & O_2 & & (R23) \\
 & Br & + & O_3 & \longrightarrow & BrO & + & O_2 & & (R24) \\
 & ClO & + & BrO & \longrightarrow & Br & + & ClOO & & (R25) \\
 & ClOO & + & M & \longrightarrow & Cl & + & O_2 & + M & (R26) \\
\hline
\text{net:} & 2\,O_3 & & & \longrightarrow & & & 3\,O_2. & & (R27)
\end{array}
$$

When the polar vortex is dynamically broken in October or November, the 'hole' is filled in by the rapid influx of ozone-rich air from lower latitudes.

Many observations show that a large amount of ozone in the lower stratosphere is destructed in Antarctic spring. The vertical column density of ozone in October sometimes becomes about a half of the historical value of about 300 Dobson units (1 Dobson unit (DU) = 1×10^{-3} atmo-cm = 2.687×10^{16} cm^{-2}) [e.g., WMO, 1991]. Some model calculations based on the observational data suggest that about 80 % of the ozone destruction rate is due to the ClO dimer catalytic cycle ((R18) - (R21)) and about 20 % is due to the coupled ClO - BrO catalytic cycle ((R23) - (R26)) [Jones *et al.*, 1989; Anderson *et al.*, 1989].

It is noteworthy that the abundance of active nitrogen (NO and NO_2) controls the efficiency of those catalytic cycles because NO_2 can convert ClO into the reservoir species

$ClONO_2$ ((R7)). The heterogeneous reactions (R13), (R14), (R16), and (R17) convert the nitrogen reservoir species $ClONO_2$ and N_2O_5 further into the reservoir species HNO_3, which is more stable nitrogen and may be removed from the stratosphere in such a way that HNO_3 trapped in the PSC particles sediments to the troposphere. All these processes result in very low concentration of active nitrogen inside the polar vortex in winter and early spring, and the ozone depletion processes become very effective. Some observations show that the low concentration of active nitrogen and the high concentration of active chlorine occur simultaneously inside the polar vortex [e.g., Kawa *et al.*, 1992].

The heterogeneous processes on the PSC particles depend on the physical and chemical properties of PSCs whose details remain uncertainty. Two major types of PSCs have been identified in Antarctica. The type I PSCs are mainly composed of nitric acid trihydrate ($HNO_3 \cdot 3H_2O$) and are formed at temperature below 195 K in the lower stratosphere. These particles are small of 0.1 - 1 μm in radii and will be little subjected to sedimentation. The type II PSCs are mainly composed of water ice with trace amount of nitric acid and are formed at temperature below 187 K. Type II particles are relatively large of 10 - 100 μm in radii and will be easily subjected to sedimentation that removes water and nitric acid from the lower stratosphere [Turco *et al.*, 1989]. Because the type I PSCs are formed at warmer temperature than the type II PSCs, the type I PSCs can appear more frequently and widely than the type II PSCs. Some laboratory measurements obtained the reaction probabilities on PSC-like surfaces for reactions (R13) to (R17) [e.g., Hanson and Ravishankara, 1991]. For example, the reaction probability of (R14) is much lower on the type I PSC surface than on the type II PSC surface. But the uncertainties of measured probabilities are still large for some reactions.

For the quantitative understanding of the Antarctic ozone depletion, it is important to know the amount of active chlorine converted from the reservoirs. Observation of HCl provides information on the extent of this conversion. The Airborne Antarctic Ozone Experiment (AAOE) observed HCl vertical column densities above the flight altitude (10 - 12 km) [Toon *et al.*, 1989; Coffey *et al.*, 1989], to exhibit that the HCl column density are smaller ($< 1 \times 10^{15}\mathrm{cm}^{-2}$) inside the vortex than outside ($2 - 3 \times 10^{15}\mathrm{cm}^{-2}$) in September. This aircraft measurement is useful to depict the spatial structure. On the other hand, a ground-based measurement is useful to show the time variation. However, there are few observations of HCl on the ground in Antarctica and the observational periods is relatively short [e.g., Liu *et al.*, 1992]. In this study, the author observed HCl vertical column densities for five months at Syowa Station (69.0°S, 39.6°E) to investigate the time variation of the partitioning of the chlorine species from winter to summer.

1.2 Stratospheric hydrogen fluoride

HF is formed after the photodissociation of chlorofluorocarbons (CFCs) in the same way as HCl. There is a possibility of natural sources of HF such as the emissions from volcanoes [e.g., Symonds *et al.*, 1988], but the contribution to the total abundance is thought to be smaller than in the case of HCl. A comparison of HCl and HF will provide some indication of the relative abundances of natural and anthropogenic halogens in the stratosphere. There are some transient reservoirs of fluorine species CF_2O and CFClO that are the intermediates during the photodissociation and subsequent reactions of CFCs [e.g., Kaye *et al.*, 1991]. These transient reservoir species are converted into more stable reservoir species HF that are not actively involved in the chemistry of the stratosphere.

A comparison of HCl and HF can indirectly examine the chemical reactivity of HCl. In addition, the stability of HF makes it possible to use as a good tracer of atmospheric motion.

In the case of solar infrared absorption spectroscopy, HF can be measured together with HCl using the same instruments. The Balloon Intercomparison Campaigns have shown that HF mixing ratios increase with altitude in the stratosphere [WMO, 1986; Mankin *et al.*, 1990]. The observed mixing ratios are about 0.1 ppbv at an altitude around 20 km increasing to about 0.5 ppbv at an altitude around 45 km. Mankin and Coffey [1983] obtained the latitudinal distribution of the stratospheric column densities of HF varying from 1.4×10^{14}cm^{-2} around the equator to 4.6×10^{14}cm^{-2} at 70°N latitude. Girard *et al.* [1983] found a minimum which is below their detection limit of 1.6×10^{14}cm^{-2} at the equator and a maximum of 3.3×10^{14}cm^{-2} at 62°N latitude. As for the long-term trend of HF, Mankin and Coffey [1983] obtained an increase rate of 12 % yr^{-1} at mid-latitudes. Rinsland *et al.* [1991] derived an increase rate of (10.9±1.1) % yr^{-1} from the ground-based observations at Kitt Peak. These increase rates are larger than those of HCl. Furthermore, Rinsland *et al.* [1991] found that HF/HCl ratio in vertical column density increased from 0.14 in May 1977 to 0.23 in June 1990, suggesting the increase of anthropogenic sources. Seasonal variations of HF are similar to those of HCl. HF vertical column density shows a maximum in early spring and a minimum in early fall with a peak-to-peak amplitude of 25 % [Rinsland *et al.*, 1991]. In addition, HF also shows short-term variability in a time scale of a day [Zander *et al.*, 1987a], but doesn't show any systematic diurnal variation. Because HF is chemically stable in the stratosphere, such variabilities are considered as a result of the planetary-scale atmospheric motion.

There are some simultaneous measurements of vertical column densities of HF and HCl in the Antarctic stratosphere [Toon *et al.*, 1989; Coffey *et al.*, 1989]. These measurements demonstrate that the HCl/HF ratio is much smaller inside the vortex than outside in September, indicating that HCl has been chemically removed inside the vortex. However, there is no report on the time variation of HF in Antarctica. In this study, the author observed the seasonal excursion of HF vertical column densities in Antarctica for the first time, to show the chemical activity of HCl.

1.3 Stratospheric nitrous oxide

N_2O is the source gas of the reactive nitrogen oxides (NO and NO_2) in the stratosphere and is an effective greenhouse gas. N_2O itself is produced principally by soil bacteria through nitrification and/or denitrification processes on which the use of nitrogen fertilizer may give an impact. There are anthropogenic productions of N_2O, especially through combustion processes. N_2O is very stable in the troposphere and is easily transported to the stratosphere. It is removed in the stratosphere mainly by photodissociation and secondarily by reaction with $O(^1D)$,

$$N_2O + h\nu \longrightarrow N_2 + O \qquad \text{(R28)}$$
$$N_2O + O(^1D) \longrightarrow NO + NO \qquad \text{(R29)}$$
$$N_2O + O(^1D) \longrightarrow N_2 + O_2. \qquad \text{(R30)}$$

Reactive nitrogen oxides are produced only through reaction (R29). The production of NO due to (R29) is estimated to make up about 20 % of the loss of N_2O [e.g., Crutzen and Schmailzl, 1983].

As a result of the ground surface source and stratospheric sink, the mixing ratio of N_2O is expected to decline with altitude in the stratosphere. Rinsland *et al.* [1982] determined the stratospheric N_2O mixing ratio profile from solar infrared absorption spectroscopy

aboard a stratospheric balloon. They reported that the mixing ratio was 264 ppbv at an altitude around 15 km decreasing to 155 ppbv around 28 km. N_2O concentration show very little geographic variation in the troposphere because of its long lifetime and thereby complete mixing. A global average concentrations was 310 ppbv in 1992 and increase rates of 0.20 - 0.34 % yr^{-1} were derived from several long-term measurements [WMO, 1991; WMO, 1994].

Like HF, N_2O is considered to be a good tracer of atmospheric motion because of its chemical inactivity. Some Antarctic measurements of the stratospheric N_2O and HF suggest that downwelling motion occurred inside the polar vortex [e.g., Toon *et al.*, 1989]. In this study, the author observed both N_2O and HF vertical column densities in Antarctica, to obtain some information on atmospheric vertical motion.

2 Instrumentation and Observation

2.1 Instrumentation

The observational technique adopted in this study is solar infrared absorption spectroscopy. The observation was carried out from the ground level and the vertical column densities of the target molecules were obtained from the measured spectra. Thermal emission of the atmosphere is negligible because the direct solar light was used as a source for absorption spectroscopy at near infrared wavelengths (2.5 to 3.9 μm).

The observational system is illustrated in Figure 2-1. The instrument consists of a servo-controlled solar-tracker with a 10 cm aperture of the optical system, a $f/8$ telescope of 13 cm diameter, a grating monochromator with a collimator of focal length 1.5 m and $f/12$ used in double-pass mode, a CaF_2 lens, an InSb detector cooled with liquid nitrogen, and a control and recording unit.

The solar-tracker follows the sun with an error less than 0.01°, which is good enough to guide the solar light stably into the monochromator. The solar-tracker was set on the roof of the building to guide the solar light into the telescope. The tracking range is between 180° and −90° in azimuth (clockwise from the north) and between −5° and 60° in elevation. It can follow the sun during almost all through daytime except for white nights in summer. The telescope forms an image of the solar disk of a 10 mm diameter on the entrance slit of the monochromator. It has an iris to match the f-number to that of the monochromator and condenses the solar spectral energy by a factor of 27. A CaF_2 beam splitter is set between the telescope and the entrance slit, and the split light is detected by a PbSe detector with a 3.4 μm band-pass filter for monitoring the apparent

fluctuation of the solar light.

The most important component of this system is a monochromator (Jobin-Yvon THR1500) with a Czerny-Turner mount and curved slits. The monochromator is equipped with a mechanically ruled grating of 300 grooves per mm and a size of 110 mm × 110 mm. The widths of the entrance and exit slits were set to be 100 μm for the HCl spectral line at 2926 cm^{-1} in wavenumber (3.418 μm in wavelength), 75 μm for the HF spectral line at 4039 cm^{-1} (2.476 μm), and 120 μm for the N_2O spectral line at 2583 cm^{-1} (3.871 μm), and the slit height was kept constant 7 mm for all spectral lines. The full-widths at half maximum of the slit function are estimated to be 0.085 cm^{-1} at 2926 cm^{-1}, 0.137 cm^{-1} at 4039 cm^{-1}, and 0.075 cm^{-1} at 2583 cm^{-1} from the theoretical value and the laboratory measurements using a 3.4 μm He-Ne laser. These wavenumber resolutions are good enough to detect one spectral line separated from others although they are not enough to measure line profiles to obtain information on the vertical distribution of trace gases. A glass filter to cut low wavelength is set in front of the entrance slit to eliminate the contamination due to the higher order diffraction. The cut-off wavelength was 2.7 μm for the HCl and N_2O spectral lines, and 1.9 μm for the HF spectral line.

The detector unit is an InSb photodiode (EG & G Judson J10D) with a detector element of 4 mm diameter and cooled with liquid nitrogen. A CaF_2 lens of 12 mm diameter with a focal length of 12 mm is set between the exit slit and the detector to collect the output light onto the detector. The signal current of the detector is converted into voltage output with a current mode preamplifier (EG & G Judson PA-9). The preamplifier output is further amplified to an order of several volts with a lock-in amplifier (NF Electronic Instruments 5600A). The chopping frequency is set at 300 Hz by means

of a motor drive controlled with phase-locked loop to reduce the hum noise and the drifts of the detector and the preamplifier. The time constant is set at 300 ms to reduce high frequency fluctuation of the signal.

A personal computer is used to control the instrument and to record the data on floppy disks with a 12 bit A/D converter. The scanning speed of the spectrometer is 2 nm per minute and the sampling time interval is 100 ms; therefore the sampling interval is 0.0028 cm^{-1} in wavenumber for the HCl spectral line, 0.0055 cm^{-1} for the HF spectral line, and 0.0022 cm^{-1} for the N_2O spectral line.

Figures 2-2 through 2-4 show examples of the observed spectra of HCl, HF, and N_2O, respectively. Signal-to-noise ratio in the spectral intensity is about 100 and varies with observational conditions. The noise is originated from electric noise, fluctuation of photon flux, and fluctuation of atmospheric transmittance.

2.2 Observation

The observation was carried out at Syowa Station (69.006° S, 39.590° E) as one of the programs of the 32nd Japanese Antarctic Research Expedition from July 31 to December 21, 1991. The instrumentation was set up in the observatory building (about 20 m above the sea level) in April, but the measurement couldn't be carried out until July because of the trouble of the instrument. Data were taken only under the clear sky because the direct solar light is necessary for the observation. The measurements were carried out on 40 clear days: 1 day in July, 8 days in August, 7 days in September, 10 days in October, 6 days in November, and 8 days in December. Only one spectrum for the HF absorption line could be measured on July 31. The measurement couldn't be carried out for one

month from mid-October to mid-November due to the absence of clear day.

The daily measurement sequence was as follows. At first the instrument measures two sets of spectra for the HCl absorption line, secondly one set of spectra for the HF absorption line and one set of spectra for the N_2O absorption line, thirdly several sets of spectra for other species (these species are not mentioned in this paper), and fourthly two sets of spectra for the HCl absorption line. The sequence was repeated as far as the solar-tracker were able to track the sun. It took 5 minutes to obtain one set of spectra, consisting of two spectrum: the forward and backward scans of the wavelength.

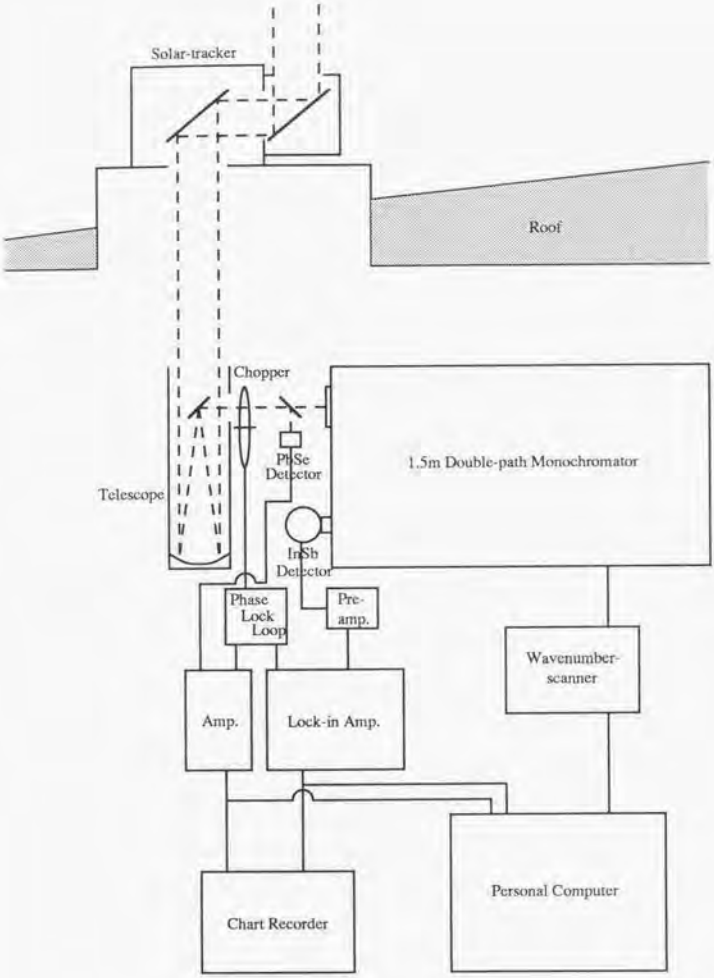

Figure 2-1. Schematic diagram of the observational system.

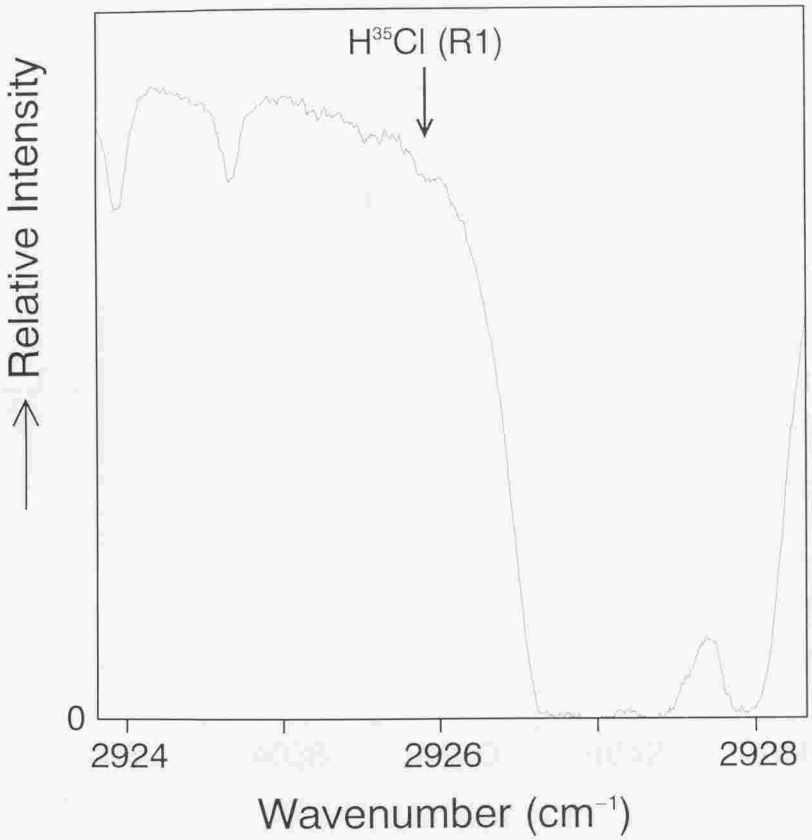

Figure 2-2. A sample of the spectra around the HCl line observed at the solar zenith angle of 73.4° on October 3, 1991.

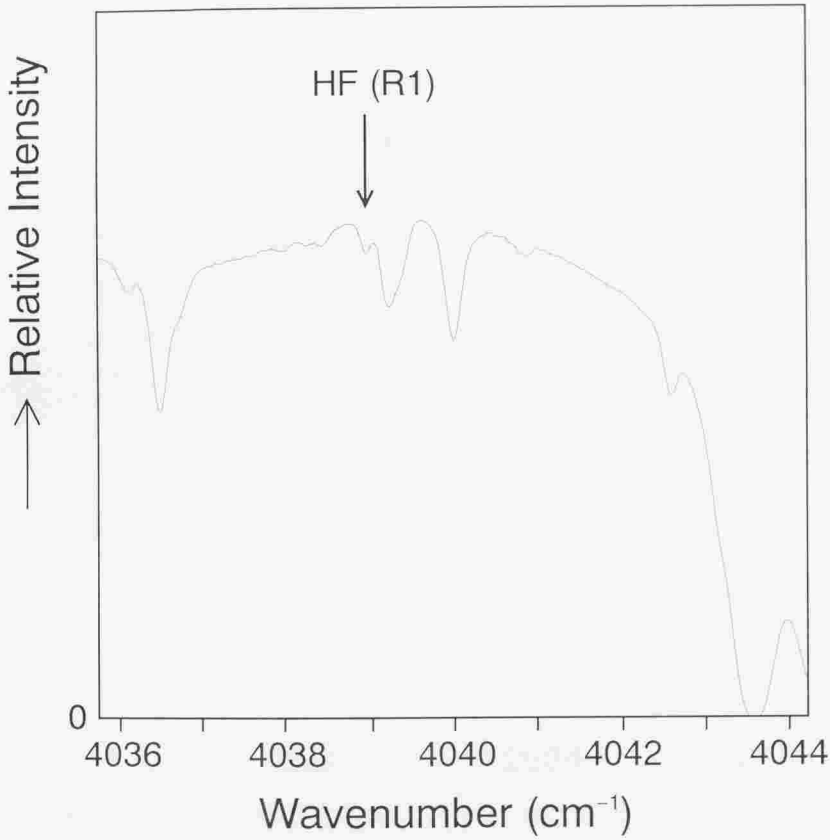

Figure 2-3. A sample of the spectra around the HF line observed at the solar zenith angle of 65.5° on October 3, 1991.

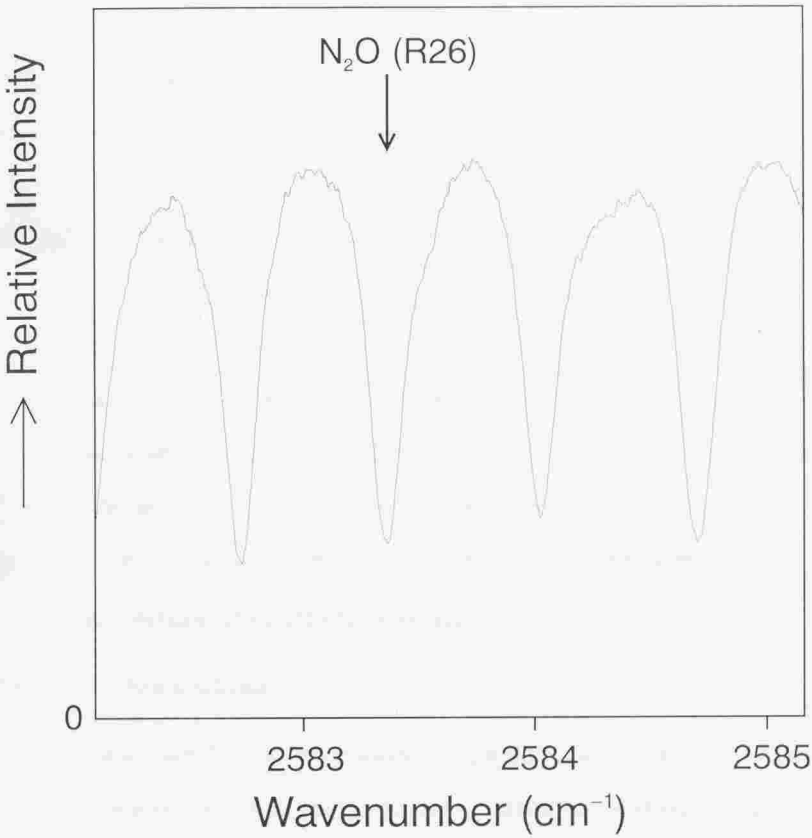

Figure 2-4. A sample of the spectra around the N_2O line observed at the solar zenith angle of 72.4° on October 3, 1991.

3 Data Analysis

The vertical column densities of HCl, HF, and N_2O were determined from the measured spectra by means of least squares fitting of the synthetic spectra that were generated with line-by-line calculations.

The calculation of the synthetic spectrum is based on a 28-layer model atmosphere for the altitude range from 0 to 48 km, assuming the vertical profiles for atmospheric temperature and pressure. Initial values were necessary for the volume mixing ratios of some atmospheric species. A Voigt profile was assumed in the calculations of molecular absorption with the database for line parameters. The synthetic spectrum thus calculated was convolved with an instrument slit function to match spectral resolution with the measured spectrum.

The synthetic spectrum is fitted to the measured spectrum by scaling the volume mixing ratio profile of the species using the least squares technique. The fitting process should be iterated once or twice to get to convergence because the convolution of the synthetic spectrum with the instrument slit function yields a non-linear effect.

3.1 Calculation of synthetic spectra

3.1.1 Calculation scheme

The transmittance $Tr(\nu)$ at the wavenumber ν (in cm^{-1}), which is the ratio of the solar light intensity observed on the ground $I(\nu)$ to that at the top of the atmosphere $I_0(\nu)$, is defined by

$$Tr(\nu) = \frac{I(\nu)}{I_0(\nu)} = \exp\{-\tau(\nu)\}, \tag{1}$$

where $\tau(\nu)$ is optical thickness and defined by

$$\tau(\nu) = \int_0^\infty \left\{ \sum_l \sigma_l(z, \nu) N_{i(l)}(z) \right\} ds. \tag{2}$$

σ_l (in cm^2) is the absorption cross section of the l-th absorption line. N_i (in molecule/cm^3) is the number density of the i-th molecule. z is height, and $\int ds$ means the integration along the optical path. Applying the 28-layer model atmosphere, $\tau(\nu)$ is rewritten as

$$\tau(\nu) = \sum_{j=1}^{28} \sum_l \sigma_{l,j}(\nu) N_{i(l),j} L_j(\chi_j), \tag{3}$$

where L_j (in cm) is the optical path length in the j-th layer and χ_j is the solar zenith angle at the lower boundary of the j-th layer.

$\sigma_{l,j}(\nu)$ in Equation (3) is expressed using the Voigt function as

$$\sigma_{l,j}(\nu) = \frac{S(l,j)}{\sqrt{\pi}\,\nu_D(l,j)} \frac{y}{\pi} \int_{-\infty}^{\infty} \frac{e^{-t^2}}{(x-t)^2 + y^2} dt, \tag{4}$$

where $S(l,j)$ [in cm^{-1}/(molecule-cm^{-2})] is the line intensity of the l-th absorption line in the j-th layer, and the dimensionless variables x and y are defined in terms of the wavenumber difference from the line center $\nu - \nu_0$, the air-broadened half-width ν_L, and $1/e$ Doppler half-width ν_D:

$$x = \frac{\nu - \nu_0(l)}{\nu_D(l,j)}, \qquad y = \frac{\nu_L(l,j)}{\nu_D(l,j)}. \tag{5}$$

The Voigt function is calculated in terms of the computational code developed by Drayson [1976]. $S(l,j)$, $\nu_L(l,j)$, and $\nu_D(l,j)$ are calculated in terms of the line parameters along with atmospheric temperature and pressure of the layer:

$$S(l,j) = S_0(l) \left\{ \frac{T_0}{T(j)} \right\}^m \exp\left[\frac{hc}{k} E''(l) \left\{ \frac{1}{T_0} - \frac{1}{T(j)} \right\} \right]. \tag{6}$$

$$\nu_L(l,j) = \left\{\frac{P(j)}{P_0}\right\}\left\{\frac{T_0}{T(j)}\right\}^{n(l)} \nu_{L0}(l) \tag{7}$$

$$\nu_D(l,j) = \nu_0(l)\sqrt{\frac{2\,k\,T(j)}{M_i\,c^2}}, \tag{8}$$

where m in Equation (6) is a coefficient for temperature dependence of the line intensity and given as

$$m = \begin{cases} 1 & \text{for linear molecules such as HCl, HF, } N_2O, CO_2, \text{ CO, and OH} \\ 3/2 & \text{for symmetric molecules such as } H_2O, O_3, CH_4, NO_2, \text{ HCHO, and } CH_3Cl. \end{cases}$$

$\nu_0(l)$, $S_0(l)$, $\nu_{L0}(l)$, $E''(l)$, and $n(l)$ are wavenumber of line center, line intensity at 296 K, air-broadened half-width at 296 K and 1013.250 hPa, energy of the lower state in cm^{-1}, and coefficient for temperature dependence of air-broadened half-width, respectively. These values are taken from the 1992 HITRAN database. h, k, and c are Planck's constant, Boltzmann's constant, and the light speed, respectively. M_i is the molecular mass of the i-th molecule. $T_0 = 296$ K, $P_0 = 1013.250$ hPa, and $T(j)$ and $P(j)$ are atmospheric temperature and pressure in the j-th layer.

$N_{i(l),j}$ in Equation (3) is calculated using the vertical profiles of volume mixing ratios together with atmospheric temperature and pressure.

In calculating $L_j(\chi_j)$ in Equation (3), sphericity of the earth is considered but refraction is neglected since the refraction effect is important only in the lower troposphere at large solar zenith angle. The error due to neglecting the refraction effect is discussed in the section 3.3.

The spectrum calculated according to Equations (1) and (3) was convolved with an instrument slit function $fs(\nu)$ to match spectral resolution with the measured spectrum.

The convolved transmittance $Trs(\nu)$ is given as

$$Trs(\nu) = \int_{-\infty}^{\infty} fs(t)\,Tr(\nu - t)dt \Big/ \int_{-\infty}^{\infty} fs(t)dt, \tag{9}$$

where $fs(\nu)$ is a triangle function with a full-width at half maximum (FWHM) of ν_S. ν_S is estimated from the theoretical values on the spectrometer characteristics and checked by the laboratory measurement of the slit function at 3.4 μm wavelength using a He-Ne laser.

3.1.2 Model atmosphere

The model atmosphere consists of 28 horizontally homogeneous layers with a thickness of 1 km from 0 km to 16 km altitudes, 2 km thickness from 16 km to 32 km, and 4 km thickness from 32 km to 48 km. The top of the atmosphere is set at the 48 km altitude, above which the airmass is less than 0.1 % of the total air mass; almost all atmospheric HCl, HF, and N_2O molecules are distributed below 48 km.

3.1.3 Vertical distributions of temperature and pressure

The vertical distributions of atmospheric temperature and pressure were observed with radiosondes by the Japan Meteorological Agency team at Syowa Station. Meteorological condition in the stratosphere changed considerably from July to December over Syowa Station, and the observation period is divided according to the profile shapes of temperature and pressure: July 31 - September 18 and September 29, September 24 and October 3 - 6, October 7 - 16, November 15 - 16, November 20 - 26, December 3 - 6, and December 14 - 21. The average profiles of temperature and pressure are determined for each group using the radiosonde data up to the altitude of about 25 km. Above about 25

km altitude, atmospheric temperature was taken from the 1972 COSPAR International Reference Atmosphere (CIRA) at 70°N and atmospheric pressure was calculated in terms of hydrostatic equilibrium.

Table 3-1 and Figure 3-1 show the atmospheric temperature and pressure profiles used in the calculation.

3.1.4 Vertical distributions of trace gases

All possible atmospheric trace species, which have absorption lines of potential influence within a wavenumber range of $\pm 5 cm^{-1}$ from the line center of $H^{35}Cl$ (R1), HF (R1), or N_2O (R26), are considered in the calculation though weak absorption lines are neglected as described in the section 3.1.5.

The HCl spectral line chosen in this study is the R(1) line of the (1-0) vibration-rotation band of $H^{35}Cl$ at $2925.8967 cm^{-1}$, around which there are absorption lines of H_2O, O_3, CH_4, NO_2, OH, HCHO, and CH_3Cl. The chosen HF line is R(1) of (1-0) vibration-rotation band at $4038.9625 cm^{-1}$, around which there are absorption lines of H_2O, N_2O, CO, CH_4, and OH. The chosen N_2O line is R(26) of $2\nu_1$ vibration-rotation band at $2583.3850 cm^{-1}$, around which there are absorption lines of H_2O, CO_2, O_3, CO, and CH_4. Therefore, twelve species are considered in the calculation: HCl, HF, N_2O, H_2O, CO_2, O_3, CO, CH_4, NO_2, OH, HCHO, and CH_3Cl.

The initial profiles of the volume mixing ratios in each layer were constructed by synthesizing the results from previous observations, observations at mid-latitudes, and model calculations [e.g., WMO, 1986; Brasseur and Solomon, 1986; Warneck, 1988; Remsberg and Russell, 1987; Brasseur *et al.*, 1990]. The ground surface data are available at Syowa

Station for CO_2 and CH_4. H_2O mixing ratios below 10 km were calculated from the atmospheric temperature and relative humidity measured with radiosondes over Syowa Station. HCl mixing ratio profiles were assumed according to seasonal variation. In particular, the winter profile represents that HCl is mostly removed between 12 and 26 km altitudes considering the heterogeneous reactions occurring on the surfaces of the PSC particles. It was used for the analysis of the measurements in August.

Table 3-2 and Figure 3-2 show the volume mixing ratio profiles used in the calculation.

3.1.5 Line parameters

The rotational line parameters of relevant atmospheric trace gases are compiled in the 1992 HITRAN database [Rothman *et al.*, 1992]. Five parameters are necessary to calculate the profile of an absorption line: wavenumber of line center in cm^{-1}, line intensity in $cm^{-1}/(molecule{\cdot}cm^{-2})$, air-broadened half-width in cm^{-1}/atm, energy of the lower state in cm^{-1}, and coefficient for temperature dependence of air-broadened half-width. Table 3-3 shows the line parameters of $H^{35}Cl$ (R1), HF (R1), and N_2O (R26).

There are 853 lines within a range of $\pm 5 cm^{-1}$ from the $H^{35}Cl$ (R1) line center. But many lines are not strong enough to interfere the $H^{35}Cl$ (R1) absorption. Those weak absorption lines are neglected to save computational time according to the following criterion. In the wavenumber range within the FWHM away from the $H^{35}Cl$ (R1) line center, i.e., $2925.8967 \pm 0.14 cm^{-1}$, the optical thickness is calculated for all lines integrating from 0 to 48 km altitudes at the solar zenith angle of both 60° and 85°. If the optical thickness of a line is less than 0.01% of the total optical thickness accumulated for all lines, then the line is neglected in this study. There remains 125 lines after this procedure.

There are 193 lines within a range of $\pm 5\text{cm}^{-1}$ away from the HF (R1) line center (two strong H_2O lines around 4045cm^{-1} are also included). Since the FWHM of the HF (R1) line is 0.14cm^{-1}, there remains 47 lines after neglecting weak absorption lines.

There are 407 lines within a range of $\pm 5\text{cm}^{-1}$ away from the N_2O (R26) line center. The FWHM is 0.20cm^{-1} for the N_2O (R26) line, but a range of $\pm 0.35\text{cm}^{-1}$ away from the line center is adopted here because N_2O is mainly distributed in the troposphere and this line is significantly collision-broadened. There remains 101 lines after neglecting weak absorption lines.

Figures 3-3 through 3-5 show examples of the synthetic spectra around $H^{35}Cl$ (R1), HF (R1), and N_2O (R26), respectively.

3.2 Spectral fitting procedure

The absolute wavenumber of the measured spectrum can be determined at the peaks of absorption lines. The optical zero level must be determined because stray light contaminates the measured spectrum. The saturated level of some strong absorption lines was located above the zero level at which null input should be observed. In this analysis, the optical zero level is determined for each measured spectrum at the saturated level of some absorption lines. For the HCl spectral region, there are a few saturated CH_4 lines around 2927cm^{-1}. There are a few saturated H_2O lines around 4044cm^{-1} for the HF spectral region. However, since there is no saturated line around the N_2O (R26) line, the same zero level as for the HCl spectrum is assumed for the N_2O spectral region.

The optical thickness is represented for the synthetic and measured spectra according

to Equation (1) as

$$\tau_{obs}(\nu) = -\ln Tr_{obs}(\nu) = -\ln\left\{\frac{I_{obs}(\nu)}{I_0(\nu)}\right\}, \tag{10}$$

$$\tau_{S,cal}(\nu) = -\ln Tr_{S,cal}(\nu). \tag{11}$$

where the subscripts *obs* and *cal* indicate those derived from observation and calculation, respectively and the subscript S indicates the value after convolution with an instrument slit function. Although $I_0(\nu)$ is an unknown value, it can be assumed to change slowly with ν because there is no significant solar absorption line in the wavenumber range concerned. Therefore, $I_0(\nu)$ can be eliminated with the highpass filtering operation.

The highpass filtering operation of the function X is defined as

$$\widehat{X} = X - Lowpass(X). \tag{12}$$

where the operation $Lowpass(X)$ is the weighted mean of X with a triangle function with a FWHM of ν_{Lp}. If ν_{Lp} is too large, then the highpass filtering operation can't eliminate a slowly varying fluctuation completely. If ν_{Lp} is too small, then the absorption feature of the molecule concerned is eliminated. In this analysis ν_{Lp} is selected to be about twice of the FWHM of the line concerned. ν_{Lp} was chosen to be 0.3 cm^{-1} for the HCl and HF retrievals and 0.4 cm^{-1} for the N_2O retrieval. The error due to the use of the highpass filtering operation will be discussed in the section 3.3.

The vertical column density of the molecule concerned is calculated in such a way that the scaling factor is determined for the assumed volume mixing ratio profile of the molecule. In each spectral region, the author determines the scaling factors for two molecular species: the molecule concerned and a predominantly interfering molecule. The volume mixing ratio profiles of other species are fixed at the initial values because

their absorptions are very weak in the wavelength region concerned. In the HCl and N_2O spectral regions, CH_4 is considered as an interfering molecule and H_2O is considered in the HF spectral region.

Let the difference of the optical thickness between the observed and calculated, $\Delta\tau(\nu)$ be

$$\Delta\tau(\nu) = \widehat{\tau_{obs}(\nu)} - \widehat{\tau_{S,cal}(\nu)}. \tag{13}$$

$\Delta\tau(\nu)$ should be due to the error of the initial profiles of mixing ratios. It is represented in terms of the scaling factor α for the molecule concerned and β for the predominantly interfering molecule as

$$\Delta\tau(\nu) = (\alpha - 1)\,\widehat{\tau_{S,cm}(\nu)} + (\beta - 1)\,\widehat{\tau_{S,im}(\nu)} + g\left(\widehat{\tau_{S,cm}(\nu)},\, \widehat{\tau_{S,im}(\nu)}\right) + \varepsilon, \tag{14}$$

where

$$\begin{aligned} \tau_{cm}(\nu) &= \sum_{j=1}^{28} \sum_{i(l)=cm} \sigma_{l,j}(\nu)\, N_{i(l),j}\, L_j(\lambda_j), \\ \tau_{im}(\nu) &= \sum_{j=1}^{28} \sum_{i(l)=im} \sigma_{l,j}(\nu)\, N_{i(l),j}\, L_j(\lambda_j). \end{aligned}$$

The subscripts cm and im indicate the concerned and predominantly interfering molecules, respectively. $g\left(\widehat{\tau_{S,cm}(\nu)}, \widehat{\tau_{S,im}(\nu)}\right)$ is a non-linear term arising from the convolution of the synthetic spectrum with the instrument slit function. ε is a measurement error. If $\Delta\tau(\nu)$ is small, then $g\left(\widehat{\tau_{S,cm}(\nu)}, \widehat{\tau_{S,im}(\nu)}\right)$ is minute. The square sum of the residuals with respect to every discrete sampling interval of ν, Res is given as

$$Res = \sum_{\nu} \left\{\Delta\tau(\nu) - (\alpha - 1)\,\widehat{\tau_{S,cm}(\nu)} - (\beta - 1)\,\widehat{\tau_{S,im}(\nu)}\right\}^2. \tag{15}$$

α and β are determined so as to minimize Res. The vertical column density of the

concerned molecule C_{cm} is calculated as

$$C_{cm} = \sum_{j=1}^{28} \alpha \, N_{cm,j} \, L_j(0). \tag{16}$$

The fitting process must be iterated because of the non-linear effect of the convolution. The iteration is repeated until $|\alpha - 1| < 0.01$. Usually only once or twice iteration is necessary because of a weak non-linearity.

Figures 3-6 through 3-8 show the examples of the fitting of the synthetic spectra to the measured ones for HCl, HF, and N_2O, respectively.

3.3 Error Analysis

Table 3-4 summerizes the estimated errors. All errors are expressed as relative uncertainties in percent in terms of vertical column densities.

There are three sources of random errors: a fitting error, an error in the optical zero level, and an error in the wavenumber.

The fitting error is evaluated from the root mean squares of residuals in the fitting of synthetic spectrum to the measured one. It comes mainly from a random fluctuation of the observed signal due to electric noises and photon fluctuations that are quantum fluctuation and fluctuation of atmospheric transmittance. This error varies largely with observational conditions such as sky clearness, solar zenith angle, column amounts of the concerned and interfering molecules. The fitting error is larger for HCl and HF than for N_2O because HCl and HF absorption features are weaker than N_2O.

The errors in determination of the optical zero level and the wavenumber are also caused by the optical/electrical noises and fluctuations, but the effects of these errors do not appear in the residuals at the fitting. They are evaluated from the sensitivity studies

on the fitting analysis by means of measured spectra. The uncertainty in determining optical zero level is 1 - 2 % of the peak of measured spectral intensities. The uncertainty in the determining wavenumber is about an order of one sampling interval that is 0.0028 cm^{-1} for the HCl spectral line, 0.0055 cm^{-1} for HF, and 0.0022 cm^{-1} for N_2O. The errors in Table 3-4 are evaluated considering these uncertainties. The error in the optical zero level becomes very large for N_2O at solar zenith angles larger than 85° because the absorption due to the N_2O (R26) line is almost saturated at the line center. Therefore, the measured spectra at solar zenith angles larger than 85° were not used in this analysis. There were six measurements at such large solar zenith angles.

There are seven sources of the systematic errors: uncertainties of the molecular spectroscopic parameters, neglect of atmospheric refraction, errors in assumed volume mixing ratio profiles, errors in assumed temperature and pressure profiles, uncertainty of the width of a slit function, use of highpass filtering operation in the fitting procedure, and incomplete convergence of iteration.

The error due to the uncertainties of molecular spectroscopic parameters was evaluated from the error codes in the HITRAN data base.

The error due to the neglect of atmospheric refraction was evaluated in terms of the difference of optical path length between the cases with atmospheric refraction and without refraction. For HCl and HF distributing mainly in the stratosphere, the error is less than 0.1 % of the vertical column densities at any solar zenith angles. For N_2O distributing mainly in the troposphere, the error is less than 1 % of the vertical column densities at solar zenith angles less than 85°. It is noted again that the measured spectra at solar zenith angles larger than 85° are not used.

In order to estimate the error due to the uncertainties of volume mixing ratio profiles, a sensitivity study was carried out on the derived vertical column density by changing profile shapes. The vertical column densities derived are not sensitive to the shapes of volume mixing ratio profiles, because the width of the slit function is much wider than those of the absorption lines occurring in the stratosphere. Only the tropospheric profile influences the shape of absorption lines. For HCl and HF, the shapes of observed absorption lines are determined mostly by the shape of a slit function because they are mainly distributed in the stratosphere although the uncertainties of volume mixing ratios are several tens %. Those errors in Table 3-4 are obtained considering a 100 % change of the tropospheric column amount of HCl or HF.

The error caused by the difference between the winter and summer profiles must be considered for HCl. The winter profile is adopted for the analyses of the spectra measured in August and the summer profile is adopted for those from September to December. But the actual HCl profile is considered to be an intermediate of the two profiles during the period from September 14 to October 16. If the winter profile is used for the analyses in the intermediate period, the derived vertical column densities become larger by about 10 %.

N_2O is distributed mainly in the troposphere, and the uncertainties of its tropospheric volume mixing ratio is less than 1 %. The uncertainties of its stratospheric volume mixing ratio is several tens %. The value given in Table 3-4 was obtained considering a 50 % change of the stratospheric column amount of N_2O.

The error due to the uncertainties of temperature and pressure profiles was also evaluated from a sensitivity study. Temperature and pressure profiles are provided for seven

groups in the observational period. The variability of temperature and pressure in one group is about 10 %. The error given in Table 3-4 was obtained considering a 10 % change of temperature and pressure.

The error due to the uncertainty of the width of a slit function was also evaluated from a sensitivity study. The width of a slit function may change by several percent when the room temperature changes by 10 K. This is because the monochromator goes out of focus due to the thermal expansion of the instrument. The value given in Table 3-4 was obtained considering a 5 % change of a width of the slit function.

The error due to the use of highpass filtering operation in the fitting procedure can be evaluated by examining fitness by means of synthetic spectra. ν_{Lp} was set to be about twice of the FWHM of the molecular line concerned. The difference between the derived and true values was found to be less than 1 %.

The error due to the incomplete convergence in the iteration procedure is 1 % because the iteration is terminated when $|\alpha - 1| < 0.01$.

Total errors are calculated as the root sum squares of individual errors. For HCl and HF, the random error is larger than the systematic error. The random error for N_2O is small but total error is not very small due to the systematic error.

Table 3-1. Atmospheric temperature and pressure profiles used in the calculation.

a. Temperature in K

Height (km)	Jul.31 - Sep.18 & Sep.29	Sep.24 & Oct.3 - 6	Oct. 7 - 16	Nov.15 - 16	Nov.20 - 26	Dec. 3 - 6	Dec.14 - 21
0	250.0	253.0	253.0	273.0	266.0	273.0	271.0
1	250.0	252.0	252.0	265.0	263.0	266.0	266.0
2	248.0	249.0	251.0	257.0	258.0	261.0	261.0
3	241.5	244.0	245.5	250.5	251.0	258.0	255.0
4	235.0	239.0	240.0	244.0	245.0	255.0	250.0
5	228.5	234.0	234.5	238.0	239.0	249.0	243.0
6	222.0	228.0	229.0	231.0	233.0	241.0	238.0
7	215.5	220.0	223.5	223.0	226.0	235.0	231.0
8	210.0	213.0	216.0	215.0	219.5	225.0	225.0
9	207.0	209.0	212.0	208.0	215.0	219.0	224.0
10	204.0	207.0	210.5	205.0	214.0	215.0	225.0
11	201.0	205.0	210.0	205.5	214.0	217.0	226.0
12	199.5	204.0	210.0	206.0	215.0	219.0	227.0
13	198.0	203.5	209.5	207.0	216.5	220.0	228.0
14	196.5	203.5	210.5	208.0	219.0	221.0	229.0
15	195.0	203.5	212.0	210.0	221.0	223.0	229.5
16	194.0	205.0	215.0	212.5	226.0	226.0	230.0
18	193.0	208.0	224.0	220.0	235.0	234.0	232.0
20	193.0	212.0	232.0	229.0	238.0	236.0	233.0
22	195.5	218.0	242.0	236.0	240.0	237.0	235.0
24	199.5	223.0	247.0	243.0	241.0	238.0	236.0
26	205.0	225.0	248.0	248.0	242.0	240.0	237.0
28	210.0	226.5	248.0	251.0	243.0	241.0	239.0
30	215.0	228.0	247.0	255.0	244.0	242.0	241.0
32	220.0	230.0	240.0	257.0	248.0	246.0	245.0
36	224.0	236.0	240.0	261.0	256.0	255.0	254.0
40	228.0	245.0	245.0	264.0	264.0	264.0	264.0
44	236.0	255.0	255.0	272.0	272.0	272.0	272.0
48	244.0	265.0	265.0	280.0	280.0	280.0	280.0

Table 3-1. (continued)

b. Pressure in hPa

Height (km)	Jul.31 - Sep.18 & Sep.29	Sep.24 & Oct.3 - 6	Oct. 7 - 16	Nov.15 - 16	Nov.20 - 26	Dec. 3 - 6	Dec.14 - 21
0	9.85E2	9.85E2	9.85E2	9.85E2	9.85E2	9.90E2	9.90E2
1	8.60E2	8.60E2	8.60E2	8.70E2	8.70E2	8.70E2	8.70E2
2	7.40E2	7.50E2	7.50E2	7.60E2	7.60E2	7.70E2	7.70E2
3	6.50E2	6.60E2	6.60E2	6.70E2	6.60E2	6.70E2	6.70E2
4	5.60E2	5.70E2	5.70E2	5.80E2	5.80E2	5.90E2	5.90E2
5	4.90E2	4.90E2	4.90E2	5.00E2	5.00E2	5.10E2	5.10E2
6	4.20E2	4.20E2	4.30E2	4.40E2	4.40E2	4.50E2	4.40E2
7	3.60E2	3.70E2	3.70E2	3.80E2	3.80E2	3.90E2	3.80E2
8	3.10E2	3.10E2	3.10E2	3.20E2	3.20E2	3.30E2	3.30E2
9	2.60E2	2.70E2	2.70E2	2.70E2	2.70E2	2.90E2	2.80E2
10	2.20E2	2.30E2	2.30E2	2.30E2	2.30E2	2.50E2	2.40E2
11	1.84E2	1.92E2	1.94E2	2.00E2	2.00E2	2.10E2	2.10E2
12	1.55E2	1.63E2	1.65E2	1.67E2	1.72E2	1.79E2	1.81E2
13	1.31E2	1.38E2	1.40E2	1.42E2	1.47E2	1.52E2	1.56E2
14	1.09E2	1.17E2	1.19E2	1.21E2	1.26E2	1.30E2	1.34E2
15	9.40E1	9.80E1	1.01E2	1.03E2	1.08E2	1.12E2	1.16E2
16	8.00E1	8.40E1	8.60E1	8.80E1	9.30E1	9.60E1	1.00E2
18	5.50E1	6.00E1	6.30E1	6.40E1	6.90E1	7.20E1	7.40E1
20	3.80E1	4.30E1	4.70E1	4.70E1	5.20E1	5.40E1	5.60E1
22	2.70E1	3.10E1	3.50E1	3.50E1	3.90E1	4.00E1	4.20E1
24	1.90E1	2.30E1	2.70E1	2.70E1	2.90E1	3.00E1	3.10E1
26	1.40E1	1.68E1	2.03E1	2.03E1	2.20E1	2.30E1	2.30E1
28	1.00E1	1.24E1	1.54E1	1.55E1	1.68E1	1.72E1	1.76E1
30	7.30E0	9.20E0	1.17E1	1.18E1	1.27E1	1.30E1	1.33E1
32	5.30E0	6.80E0	8.90E0	9.00E0	9.60E0	9.80E0	1.01E1
36	2.90E0	3.80E0	5.00E0	5.40E0	5.60E0	5.70E0	5.90E0
40	1.60E0	2.20E0	2.90E0	3.20E0	3.30E0	3.40E0	3.50E0
44	0.89E0	1.25E0	1.67E0	1.92E0	2.00E0	2.05E0	2.10E0
48	0.50E0	0.74E0	0.99E0	1.17E0	1.22E0	1.25E0	1.28E0

Table 3-2. Initial volume mixing ratio profiles used in the calculation.

Height (km)	HCl summer	HCl winter	HF	N_2O	H_2O	CO_2	O_3
0 - 1	3.50E-11	3.50E-11	1.00E-12	3.10E-07		3.53E-04	3.00E-08
1 - 2	3.50E-11	3.50E-11	1.00E-12	3.10E-07		3.53E-04	3.50E-08
2 - 3	3.50E-11	3.50E-11	1.00E-12	3.10E-07		3.53E-04	4.00E-08
3 - 4	3.50E-11	3.50E-11	1.00E-12	3.10E-07		3.53E-04	4.50E-08
4 - 5	3.50E-11	3.50E-11	1.00E-12	3.10E-07		3.53E-04	5.00E-08
5 - 6	3.50E-11	3.50E-11	1.00E-12	3.10E-07		3.53E-04	6.00E-08
6 - 7	3.50E-11	3.50E-11	1.00E-12	3.10E-07		3.53E-04	8.00E-08
7 - 8	3.50E-11	3.50E-11	1.00E-12	3.10E-07		3.53E-04	1.00E-07
8 - 9	3.50E-11	3.50E-11	1.00E-12	3.10E-07		3.53E-04	1.40E-07
9 - 10	3.50E-11	3.50E-11	1.00E-12	3.10E-07		3.53E-04	2.00E-07
10 - 11	3.50E-11	3.50E-11	1.00E-12	3.10E-07	1.90E-05	3.53E-04	2.80E-07
11 - 12	3.50E-11	3.50E-11	1.00E-12	3.04E-07	1.40E-05	3.53E-04	4.00E-07
12 - 13	2.60E-10	1.00E-12	2.00E-12	2.98E-07	1.00E-05	3.53E-04	5.00E-07
13 - 14	4.60E-10	1.00E-12	4.40E-12	2.92E-07	7.90E-06	3.53E-04	8.00E-07
14 - 15	8.50E-10	1.00E-12	1.10E-11	2.86E-07	5.90E-06	3.53E-04	1.00E-06
15 - 16	1.50E-09	1.00E-12	3.00E-11	2.80E-07	4.50E-06	3.53E-04	1.20E-06
16 - 18	1.80E-09	1.00E-12	1.00E-10	2.50E-07	4.60E-06	3.53E-04	1.60E-06
18 - 20	2.00E-09	1.00E-12	2.00E-10	2.20E-07	4.80E-06	3.53E-04	2.00E-06
20 - 22	2.15E-09	1.00E-12	3.60E-10	2.10E-07	5.00E-06	3.53E-04	2.40E-06
22 - 24	2.30E-09	1.00E-12	5.40E-10	1.90E-07	5.10E-06	3.53E-04	3.00E-06
24 - 26	2.45E-09	1.00E-12	7.60E-10	1.75E-07	5.20E-06	3.53E-04	4.00E-06
26 - 28	2.60E-09	1.60E-11	9.10E-10	1.60E-07	5.10E-06	3.53E-04	6.00E-06
28 - 30	2.75E-09	2.75E-09	1.05E-09	1.45E-07	5.10E-06	3.53E-04	6.50E-06
30 - 32	2.80E-09	2.80E-09	1.20E-09	1.30E-07	5.00E-06	3.53E-04	6.50E-06
32 - 36	2.85E-09	2.85E-09	1.40E-09	1.00E-07	5.00E-06	3.53E-04	7.00E-06
36 - 40	2.90E-09	2.90E-09	1.60E-09	6.00E-08	5.00E-06	3.53E-04	7.00E-06
40 - 44	2.95E-09	2.95E-09	1.80E-09	2.50E-08	5.00E-06	3.53E-04	7.00E-06
44 - 48	3.00E-09	3.00E-09	2.00E-09	1.00E-08	5.00E-06	3.53E-04	6.00E-06

H_2O mixing ratios below 10 km are calculated from the temperature and relative humidity measured by radiosondes over Syowa Station.

Table 3-2. (continued)

Height (km)	CO	CH_4	NO_2	OH	HCHO	CH_3Cl
0 - 1	6.00E-08	1.69E-06	1.50E-11	1.00E-13	2.00E-10	6.00E-10
1 - 2	6.00E-08	1.69E-06	2.00E-11	1.00E-13	2.00E-10	6.00E-10
2 - 3	6.00E-08	1.69E-06	3.00E-11	1.00E-13	1.00E-10	6.00E-10
3 - 4	6.00E-08	1.68E-06	3.50E-11	1.00E-13	1.00E-10	6.00E-10
4 - 5	6.00E-08	1.68E-06	4.00E-11	1.00E-13	1.00E-10	6.00E-10
5 - 6	6.00E-08	1.68E-06	5.00E-11	1.00E-13	1.00E-10	5.90E-10
6 - 7	6.00E-08	1.67E-06	6.00E-11	1.00E-13	8.00E-11	5.80E-10
7 - 8	6.00E-08	1.67E-06	1.00E-10	1.00E-13	6.00E-11	5.60E-10
8 - 9	6.00E-08	1.66E-06	1.50E-10	1.00E-13	4.00E-11	5.40E-10
9 - 10	6.00E-08	1.66E-06	3.40E-10	1.00E-13	4.00E-11	5.30E-10
10 - 11	5.40E-08	1.65E-06	3.40E-10	1.00E-13	4.00E-11	5.20E-10
11 - 12	4.90E-08	1.65E-06	3.35E-10	1.00E-13	4.00E-11	5.00E-10
12 - 13	4.40E-08	1.59E-06	3.30E-10	1.00E-13	3.00E-11	4.80E-10
13 - 14	3.90E-08	1.52E-06	3.30E-10	1.30E-13	3.00E-11	4.60E-10
14 - 15	3.40E-08	1.45E-06	3.50E-10	1.50E-13	3.00E-11	4.50E-10
15 - 16	3.00E-08	1.38E-06	3.80E-10	2.00E-13	3.00E-11	4.20E-10
16 - 18	2.40E-08	1.24E-06	5.00E-10	3.00E-13	3.00E-11	3.90E-10
18 - 20	2.00E-08	1.10E-06	9.00E-10	4.00E-13	3.00E-11	3.50E-10
20 - 22	1.60E-08	1.00E-06	1.50E-09	8.00E-13	3.00E-11	2.00E-10
22 - 24	1.30E-08	9.00E-07	3.00E-09	1.60E-12	3.00E-11	1.00E-10
24 - 26	1.00E-08	8.00E-07	4.00E-09	4.00E-12	3.00E-11	5.00E-11
26 - 28	1.10E-08	7.30E-07	5.00E-09	8.00E-12	3.00E-11	3.00E-11
28 - 30	1.20E-08	6.60E-07	6.00E-09	1.00E-11	3.00E-11	1.00E-11
30 - 32	1.30E-08	6.00E-07	7.00E-09	2.00E-11	3.00E-11	7.00E-12
32 - 36	1.60E-08	5.00E-07	4.00E-09	7.00E-11	3.00E-11	5.00E-12
36 - 40	1.90E-08	4.00E-07	3.00E-09	2.00E-10	3.00E-11	3.00E-12
40 - 44	2.30E-08	3.00E-07	1.50E-09	6.00E-10	3.00E-11	2.00E-12
44 - 48	2.80E-08	2.50E-07	1.00E-09	1.00E-09	3.00E-11	1.00E-12

Table 3-3. Line parameters of the $H^{35}Cl$ (R1), HF (R1), and N_2O (R26).

Molecule	ν_0	S_0	ν_{L0}	E''	n
$H^{35}Cl$ (R1)	2925.896675	4.194E-19	0.0793	20.8782	0.76
HF (R1)	4038.962500	2.369E-18	0.0895	41.1110	0.51
N_2O (R26)	2583.385000	1.585E-20	0.0720	294.0589	0.80

ν_0 : Wavenumber of line center (cm^{-1})
S_0 : Line intensity at 296 K [cm^{-1}/(molecule-cm^{-2})]
ν_{L0} : Air-broadened half-width at 296 K (cm^{-1}/atm)
E'' : Energy of the lower state (cm^{-1})
n : Coefficient for temperature dependence of air-broadened half-width

Table 3-4. Estimated Errors

Error source	HCl (%)	HF (%)	N_2O (%)
Random error			
Fitting error	10 - 40	5 - 25	1 - 3
Determination of optical zero level	2 - 3	1 - 3	2 - 4
Determination of wavenumber	1 - 2	1 - 3	1 - 2
Systematic error			
Uncertainties of the molecular spectroscopic parameters	2	5	Undefined
Neglect of atmospheric refraction	0.1	0.1	1
Errors in assumed volume mixing ratio profiles	5(10)*	1.5	3
Errors in assumed temperature and pressure profiles	2	3	2
Uncertainty of the width of a slit function	7	10	7
Use of highpass filtering operation	1	1	1
Incomplete convergence of iteration	1	1	1
Total error	14 - 41	13 - 28	9 - 10

* The value in the parentheses is for the measurements from September 14 to October 16.

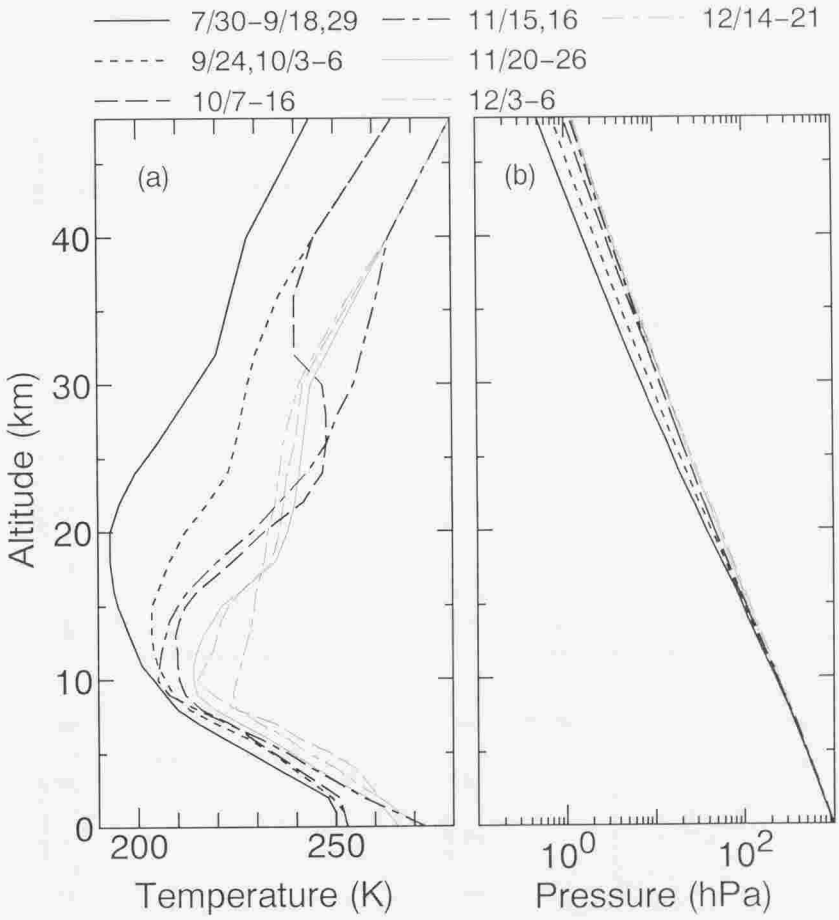

Figure 3-1. Atmospheric temperature and pressure profiles used in the calculation.

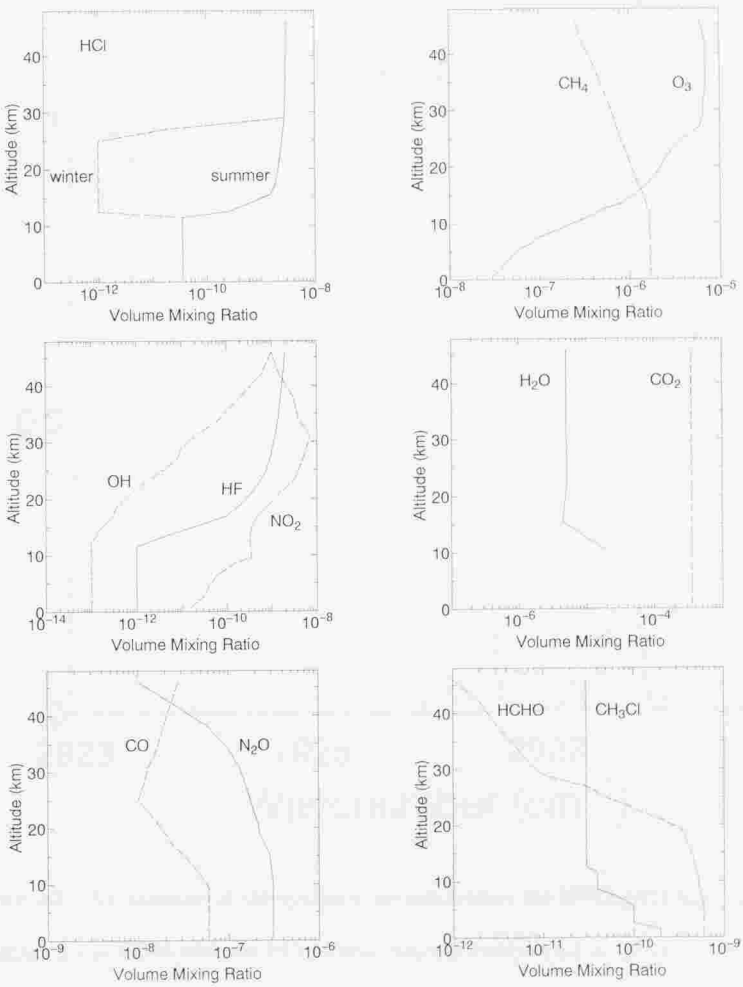

Figure 3-2. Initial volume mixing ratio profiles used in the calculation.

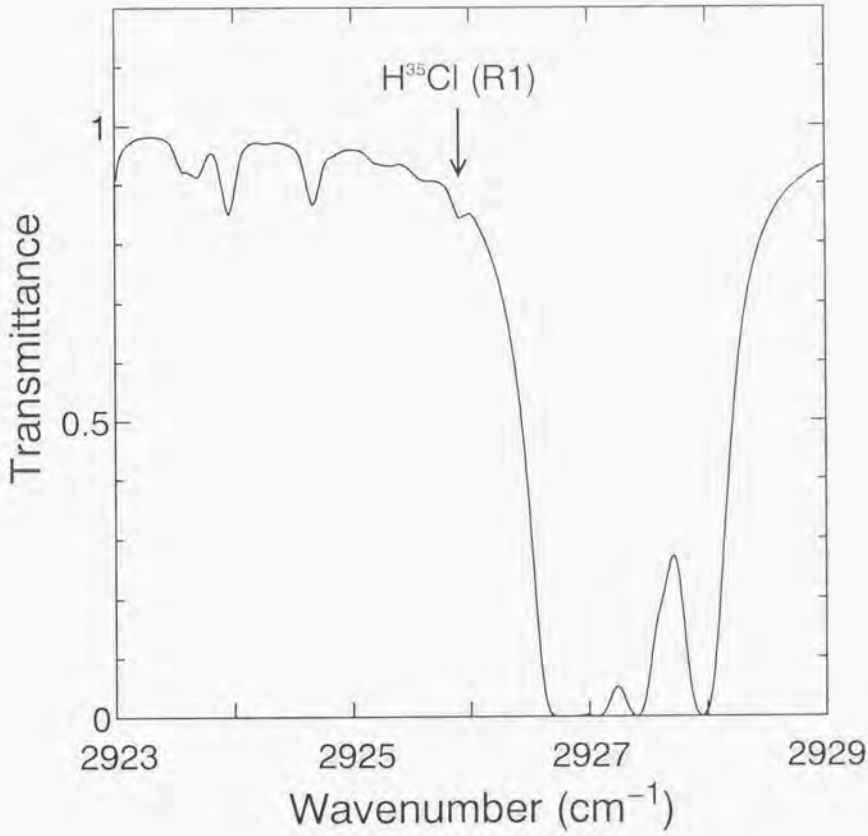

Figure 3-3. An example of the synthetic spectra around the $H^{35}Cl$ (R1) line. This spectrum is calculated with the HCl vertical column density of $5.8 \times 10^{15} cm^{-2}$ and the solar zenith angle of 60°.

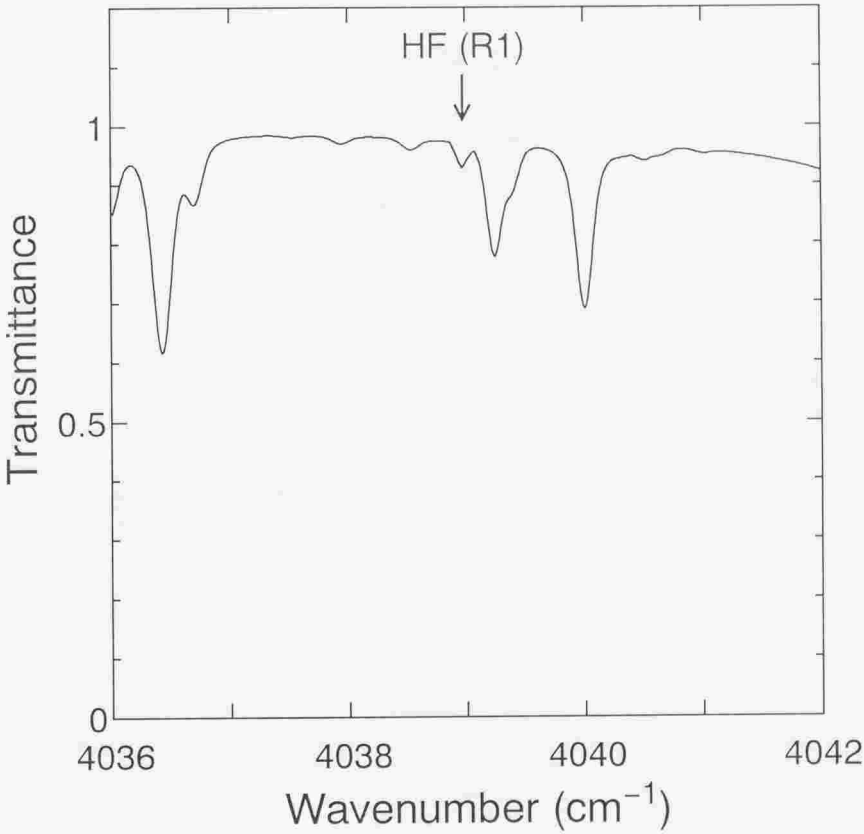

Figure 3-4. An example of the synthetic spectra around the HF (R1) line. This spectrum is calculated with the HF vertical column density of 9.2×10^{14}cm^{-2} and the solar zenith angle of 60°.

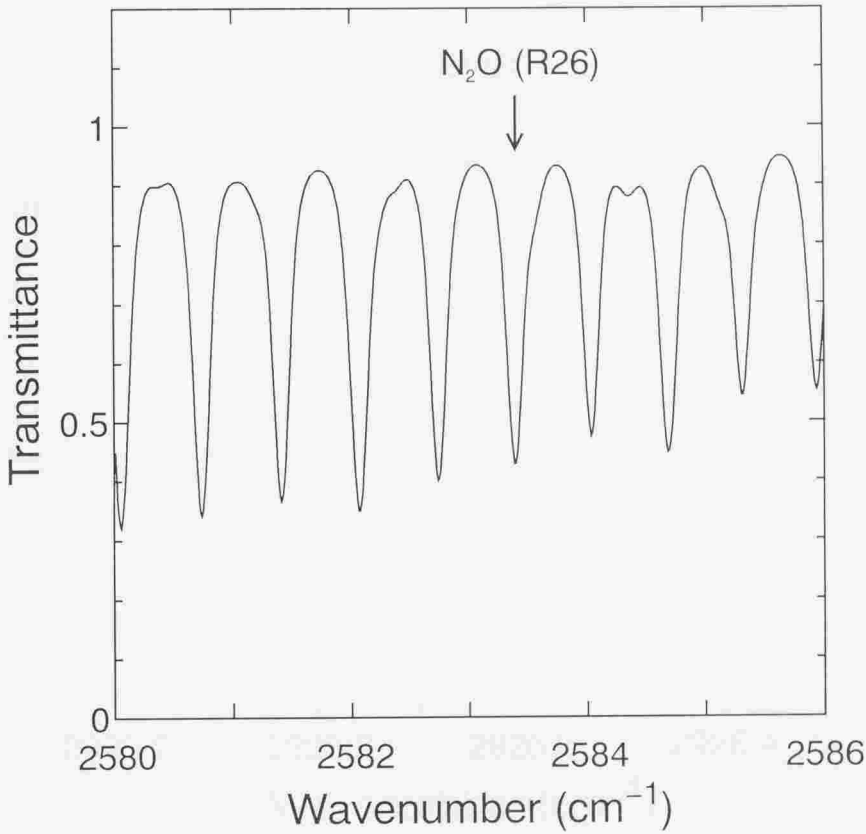

Figure 3-5. An example of the synthetic spectra around the N_2O (R26) line. This spectrum is calculated with the N_2O vertical column density of $6.4 \times 10^{18} cm^{-2}$ and the solar zenith angle of 60°.

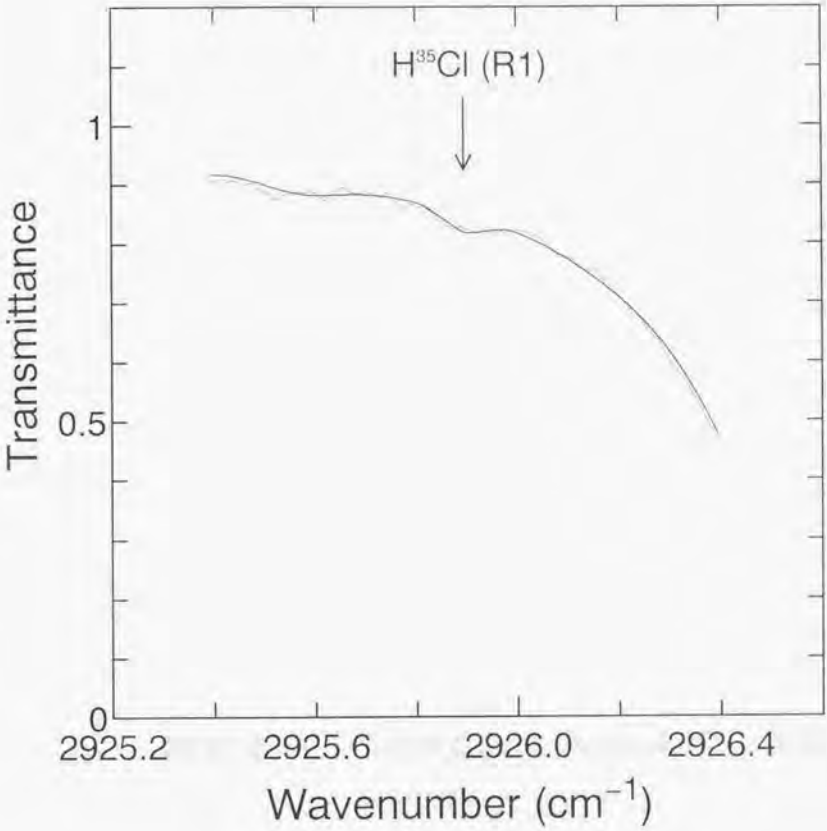

Figure 3-6. An example of the fitting of the synthetic spectrum to the measured one for HCl. The measured spectrum was obtained at the solar zenith angle of 73.35° on October 3, 1991. The derived HCl vertical column density is $(2.69 \pm 0.57) \times 10^{15} cm^{-2}$.

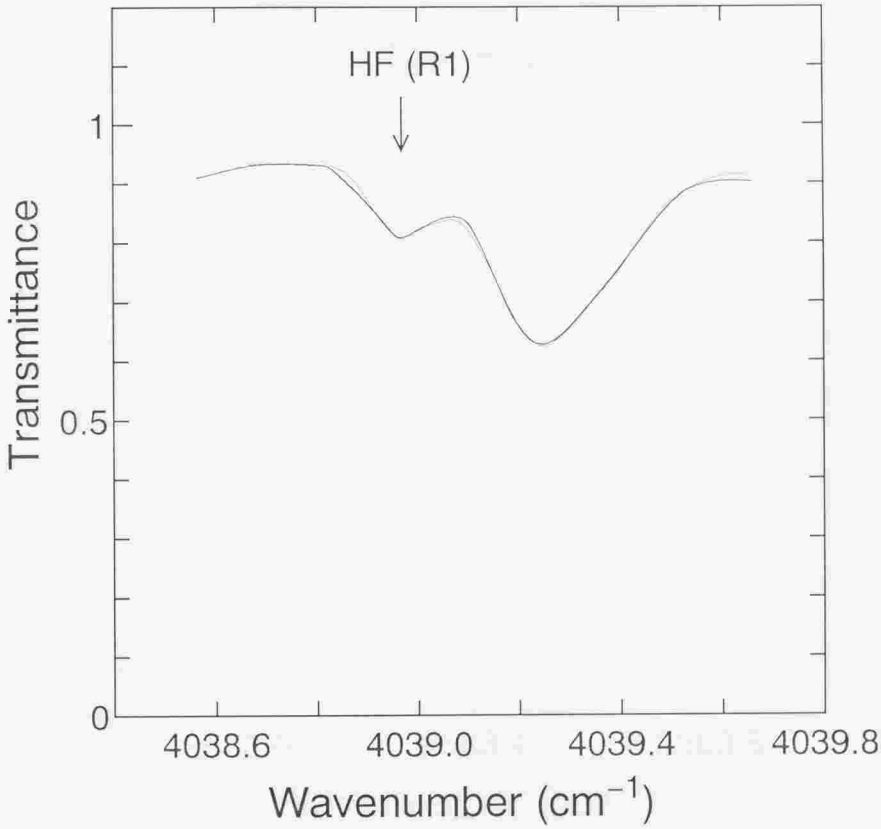

Figure 3-7. An example of the fitting of the synthetic spectrum to the measured one for HF. The measured spectrum was obtained at the solar zenith angle of 83.50° on August 14, 1991. The derived HF vertical column density is $(1.49 \pm 0.19) \times 10^{15}\text{cm}^{-2}$.

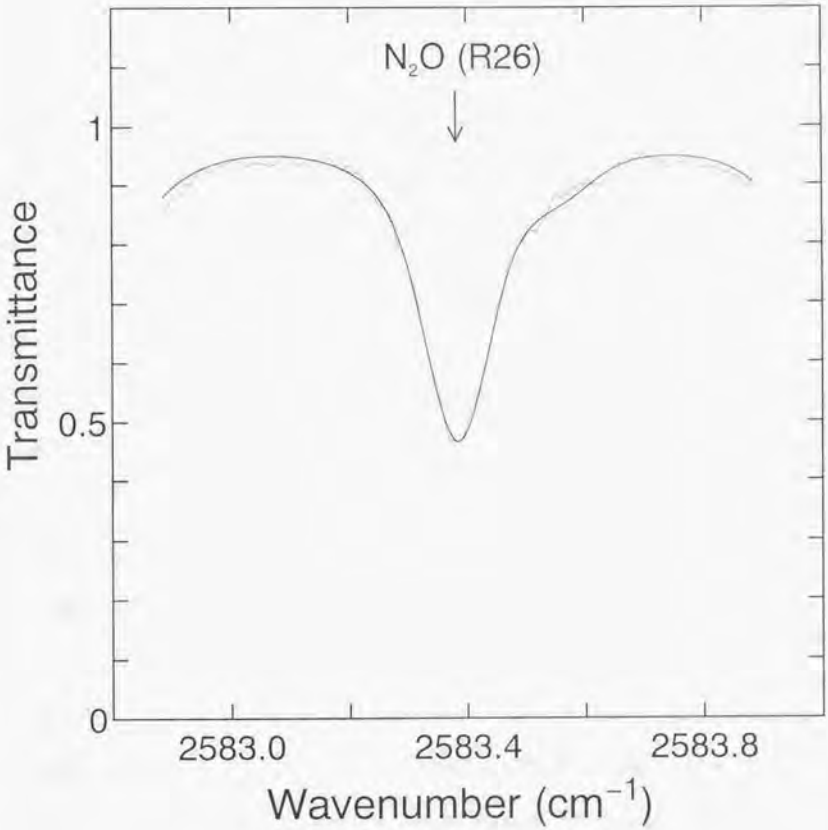

Figure 3-8. An example of the fitting of the synthetic spectrum to the measured one for N_2O. The measured spectrum was obtained at the solar zenith angle of 48.98° on November 22, 1991. The derived N_2O vertical column density is $(6.63 \pm 0.65) \times 10^{18} cm^{-2}$.

4 Observational Results

Table 4-1 provides all the data of HCl, HF, and N_2O vertical column densities measured at Syowa Station from July 31 to December 21, 1991. The errors are calculated as the root sum squares of individual errors discussed in the section 3.3. Significant diurnal variations were not found by this observation for these three species as expected from the fact that they are photochemically inactive. Therefore, discussions in the following sections are based on daily averaged vertical column densities.

Figure 4-1 shows temporal variation of daily averaged HCl vertical column densities from August to December 1991. The error bars indicate the daily average of observation errors. HCl vertical column densities are found to be $(1.65\pm0.43) \times 10^{15}\mathrm{cm}^{-2}$ in August, then increase gradually with time until mid-October, and attain to $(6.07\pm1.20) \times 10^{15}\mathrm{cm}^{-2}$ in November and in December. Day-to-day variations are mostly within observation errors.

The observed column density of HCl is compared with those obtained by other observations. The observed seasonal variation is similar to that observed at McMurdo Station (78°S, 169°E) in 1989 [Liu *et al.*, 1992] which shows that HCl vertical column density increased from $1 \times 10^{15}\mathrm{cm}^{-2}$ in early September to $7 \times 10^{15}\mathrm{cm}^{-2}$ in late October. The HCl data are also available from the Airborne Antarctic Ozone Experiment (AAOE) carried out in August and September 1987 [Toon *et al.*, 1989; Coffey *et al.*, 1989], showing HCl vertical column densities to be less than $1 \times 10^{15}\mathrm{cm}^{-2}$ above the flight altitude (10 - 12 km) inside the polar vortex. HCl vertical column density below 12 km altitude can be estimated from observations at mid-latitudes. HCl vertical column density at Kitt Peak

(altitude 2.09 km; 31.9°N) was 1.8×10^{15}cm^{-2} in 1980 [Rinsland *et al.*, 1991] and HCl vertical column density above $\sim$ 12 km altitude at 30°N was 1.0×10^{15}cm^{-2} according to airborne measurements from 1978 to 1982 [Mankin and Coffey, 1983]. From these results, HCl vertical column density between the ground surface and 12 km altitude is estimated to be about 1×10^{15}cm^{-2}. Therefore, HCl vertical column densities from the ground surface inside the polar vortex were less than 2×10^{15}cm^{-2}, which agrees with the winter average value of $(1.65 \pm 0.43) \times 10^{15}$cm^{-2} obtained in this study. The summer HCl column density of $(6.07 \pm 1.20) \times 10^{15}$cm^{-2} is larger than that observed at 60°S in 1980 by Girard *et al.* [1983]. Their observed HCl vertical column density was 2.7×10^{15}cm^{-2} above the flight altitude (11.5 km) and its corresponding value from the ground surface was 3.7×10^{15}cm^{-2}. However, considering increasing rate of 5 % yr^{-1} of HCl column density [e.g., Mankin and Coffey, 1983], 3.7×10^{15}cm^{-2} in 1980 corresponds to 6.3×10^{15}cm^{-2} in 1991 and agrees with the result of this study.

Figure 4-2 shows temporal variations of daily averaged HF and N_2O vertical column densities from July to December 1991. The error bars are calculated in the same way as HCl. HF and N_2O are considered as good tracers of atmospheric motion because they are photochemically inactive. HF and N_2O vertical column densities didn't show any meaningful seasonal variations from winter to summer in contrast to HCl vertical column density. They are found to be $(1.31 \pm 0.25) \times 10^{15}$cm^{-2} and $(5.98 \pm 0.31) \times 10^{18}$cm^{-2}, respectively. This implies that the variation of vertical transport between winter and summer is insignificant.

The observed column densities of HF and N_2O are compared with those from other observations. The HF vertical column density of $(1.31 \pm 0.25) \times 10^{15}$cm^{-2} is similar to

those observed in the AAOE campaign [Toon *et al.*, 1989; Coffey *et al.*, 1989] whose values were 0.8 - 1.6 $\times$ $10^{15}cm^{-2}$ above the flight altitude. These values can be representative of vertical column densities from the ground surface because almost all HF molecules are distributed in the stratosphere. The N_2O vertical column density of (5.98$\pm$0.31) $\times$ $10^{18}cm^{-2}$ is similar to 5.9 $\times$ $10^{18}cm^{-2}$ observed at Syowa Station in 1983 [Makino *et al.*, 1986] and is smaller than 6.48 $\times$ $10^{18}cm^{-2}$ observed at Tsukuba, Japan in 1983 [Muramatsu *et al.*, 1984] and (6.7$\pm$0.3) $\times$ $10^{18}cm^{-2}$ observed by the author in Tokyo, Japan in 1989. Since N_2O is mainly distributed in the troposphere with little geographic variation and the tropopause is located lower altitudes in Antarctica than in mid-latitudes, the tropospheric column density of N_2O is smaller in Antarctica. Consequently, N_2O vertical column density is smaller at Syowa Station than in Japan.

Day-to-day variation that shows decrease in October and December was observed in HF vertical column density, but N_2O vertical column density remained constant in October and December. HCl vertical column also decreased in December. These decreases represent transport of air mass from lower latitudes because the latitudinal distribution of HF and HCl shows an increase with latitude but N_2O shows little variation with latitude. Actually in the case of October, Syowa Station was located outside the polar vortex (it will be discussed in the section 5.1) and covered with the air mass of lower latitude origin. HF and HCl vertical column densities may be decreased due to upwelling motion; however, at the same time it must cause an increase of N_2O vertical column density. Consequently, this is not the case.

HCl/HF vertical column density ratio is a good indicator of the chemical conversion of HCl to other chlorine species. Since both HCl and HF are mainly produced from CFCs

and are relatively chemically stable. HCl/HF ratio normally does not show a significant variation with place [Mankin and Coffey, 1983]. HCl/HF ratio changes only if HCl changes chemically because HF is quite stable and almost independent of stratospheric chemistry. Figure 4-3 shows the temporal variation of HCl/HF vertical column density ratios from August to December 1991. The ratios were calculated from daily averaged HCl and HF vertical column densities on the same day, and the error bars indicate uncertainties calculated from those of daily averaged HCl and HF vertical column densities. The average of HCl/HF ratios was 4.8 in November and December as indicated by dashed line, and it agrees with the values of 4 - 5 observed in mid-latitudes [Rinsland *et al.*, 1991]. HCl/HF ratios were significantly smaller in winter than in summer, suggesting that HCl was chemically removed during winter.

The difference of HCl vertical column density between winter and summer amounts to $(4.4\pm1.6) \times 10^{15}\mathrm{cm}^{-2}$. Although the author couldn't observe HCl vertical column density before August, HCl vertical column density in the beginning of winter is expected to be nearly equal to that in summer. In the observation at mid-latitude, the seasonal variation of HCl vertical column density shows a maximum in early spring and a minimum in early fall with a peak-to-peak amplitude of about 10 % [Rinsland *et al.*, 1991; Zander *et al.*, 1987b]. If the seasonal variation from summer to fall at high-latitude is similar to that at mid-latitude, then HCl vertical column density in the beginning of winter is nearly equal to that in summer. Consequently, the amount of removal of HCl during winter is expected to be nearly equal to $(4.4\pm1.6) \times 10^{15}\mathrm{cm}^{-2}$. This is obviously larger than a half of the vertical column density in summer. It is quite difficult to explain such a large removal by means of gas phase chemistry, in which HCl is mainly removed through

the reactions with OH and O (reactions (R11) and (R12)), because these reactions are slow particularly in the lower stratosphere where atmospheric HCl is mostly distributed. HCl is supposed to be removed through heterogeneous reactions on the surfaces of the polar stratospheric cloud (PSC) particles in the lower stratosphere [e.g., Solomon, 1990; Granier and Brasseur, 1992]. There is a possibility that HCl is removed through trapping on the surfaces of PSC particles. However, there have been few quantitative discussions on HCl removal during polar night. Figure 4-4 shows the initial HCl vertical profiles of number density and volume mixing ratio for summer used in the analysis (the same as in Figure 3-2). HCl vertical column density in the altitude region between 12 and 25 km where PSCs appear [e.g., Solomon, 1990] is $4.1 \times 10^{15}\mathrm{cm}^{-2}$ according to this profile. The observed removal of $(4.4 \pm 1.6) \times 10^{15}\mathrm{cm}^{-2}$ implies that almost all HCl in the altitude region 12 - 25 km should be converted into other chlorine species during polar night.

Table 4-1. Observed vertical column densities.

a. HCl

Date (year, month, day)	Time (45°EMT)	Solar zenith angle (degree)	Vertical column density ($10^{15}cm^{-2}$)
1991 Aug. 4	11:38	86.80	1.46 ± 0.48
	11:55	86.50	1.37 ± 0.62
	13:10	86.70	2.07 ± 0.31
	13:26	87.00	1.44 ± 0.28
	13:28	87.00	1.15 ± 0.30
Aug. 14	9:32	89.00	1.28 ± 0.52
	10:29	86.10	0.74 ± 0.35
	12:25	83.50	1.60 ± 0.26
Aug. 18	9:49	86.76	1.35 ± 0.43
	10:24	85.00	1.30 ± 0.49
	10:26	84.92	1.74 ± 0.47
	12:59	82.42	1.28 ± 0.75
	13:01	82.44	1.37 ± 0.58
	13:05	82.50	2.63 ± 1.06
	13:08	82.55	1.64 ± 1.07
	13:57	83.80	2.12 ± 0.55
Aug. 21	9:11	88.07	1.43 ± 0.30
	11:01	82.59	1.75 ± 0.48
	11:04	82.50	1.31 ± 0.35
	11:06	82.44	1.24 ± 0.34
	11:09	82.35	1.67 ± 0.38
	12:12	81.30	1.39 ± 0.43
	12:14	81.30	1.70 ± 0.44
	12:17	81.25	1.39 ± 0.34
	12:19	81.24	1.31 ± 0.25
	13:46	82.47	1.48 ± 0.29
	13:50	82.59	1.72 ± 0.49
	14:44	84.81	2.00 ± 0.29
	14:47	84.96	1.37 ± 0.38
	14:49	85.06	1.59 ± 0.28
	14:52	85.22	1.67 ± 0.43
Aug. 25	12:17	79.89	1.90 ± 0.70
	12:20	79.88	2.01 ± 0.52
	12:23	79.88	1.61 ± 0.69
	12:25	79.88	1.81 ± 0.88
Aug. 28	9:55	83.00	2.95 ± 1.12
	10:25	81.53	2.91 ± 0.99

Table 4-1. (continued)

Date (year, month, day)	Time (45°EMT)	Solar zenith angle (degree)	Vertical column density ($10^{15}cm^{-2}$)
1991 Aug. 28	10:29	81.35	1.84 ± 0.76
	11:43	79.16	1.53 ± 0.69
	11:51	79.05	1.73 ± 0.85
	11:54	79.01	2.09 ± 0.85
	12:17	78.84	1.94 ± 0.90
	12:20	78.84	2.46 ± 0.60
	12:23	78.84	1.09 ± 0.76
	12:26	78.84	1.90 ± 0.69
Aug. 29	9:03	85.82	1.47 ± 0.56
	9:06	85.62	0.97 ± 0.76
Aug. 30	8:44	86.79	1.58 ± 0.57
	8:47	86.58	1.17 ± 0.62
	8:51	86.29	1.18 ± 0.62
	8:54	86.08	1.32 ± 0.66
	10:16	81.22	2.13 ± 0.47
	10:19	81.08	1.69 ± 0.44
	10:21	81.00	1.97 ± 0.65
	10:24	80.80	1.75 ± 0.51
Sep. 14	9:35	77.70	1.21 ± 0.35
	9:38	77.52	2.11 ± 0.50
	9:41	77.30	2.02 ± 0.41
	9:43	77.20	2.30 ± 0.38
Sep. 15	14:50	76.69	2.15 ± 0.46
	14:53	76.86	0.97 ± 0.54
	14:56	77.04	1.74 ± 0.30
	14:58	77.15	1.67 ± 0.40
	15:46	80.30	0.64 ± 0.55
	15:49	80.51	1.38 ± 0.44
	15:52	80.73	2.27 ± 0.50
	15:54	80.88	1.27 ± 0.50
	16:28	83.48	1.82 ± 0.36
	16:31	83.72	1.92 ± 0.56
Sep. 16	11:42	72.03	1.10 ± 0.53
	11:45	71.99	1.25 ± 0.40
	11:48	71.95	1.51 ± 0.45
	11:50	71.93	1.91 ± 0.44
	12:51	72.01	2.00 ± 0.53

Table 4-1. (continued)

Date (year, month, day)	Time (45°EMT)	Solar zenith angle (degree)	Vertical column density ($10^{15}cm^{-2}$)
1991 Sep. 16	12:54	72.05	1.40 ± 0.78
	12:57	72.10	0.96 ± 0.74
	13:00	72.15	1.38 ± 0.55
	13:54	73.66	1.19 ± 0.70
	13:57	73.77	1.46 ± 0.65
Sep. 17	10:48	73.00	1.67 ± 0.33
	10:51	72.89	1.62 ± 0.46
	10:56	72.73	1.18 ± 0.27
	10:59	72.63	1.71 ± 0.55
Sep. 18	10:00	74.71	1.97 ± 0.33
	10:03	74.56	1.76 ± 0.36
	10:06	74.40	1.99 ± 0.34
	10:09	74.30	2.97 ± 0.47
	10:59	72.24	2.07 ± 0.45
Sep. 24	12:55	69.02	2.31 ± 0.83
	12:58	69.07	2.21 ± 0.55
	13:01	69.13	2.86 ± 0.66
	13:04	69.19	2.56 ± 0.62
Sep. 29	9:31	71.98	2.96 ± 0.92
	9:33	71.85	2.19 ± 0.85
	9:36	71.67	2.00 ± 1.03
	10:35	68.72	3.12 ± 0.63
	10:37	68.64	3.90 ± 0.75
	16:53	80.83	3.83 ± 0.56
	16:56	81.08	3.12 ± 0.43
Oct. 3	8:47	73.35	2.69 ± 0.57
	8:50	73.13	2.46 ± 0.49
	8:52	72.99	2.86 ± 0.48
	8:55	72.77	3.31 ± 0.41
	9:41	69.79	2.85 ± 0.50
	9:43	69.68	2.82 ± 0.39
	9:47	69.45	3.05 ± 0.81
	9:50	69.28	3.87 ± 0.43
	12:16	65.20	3.23 ± 0.57
	12:19	65.20	3.82 ± 0.63
	13:00	65.68	3.12 ± 0.70
	13:02	65.72	4.53 ± 0.48

Table 4-1. (continued)

Date (year, month, day)	Time (45°EMT)	Solar zenith angle (degree)	Vertical column density ($10^{15}cm^{-2}$)
1991 Oct. 3	13:05	65.79	4.20 ± 0.76
	13:07	65.83	3.72 ± 0.75
Oct. 4	10:59	65.90	2.79 ± 0.59
	11:02	65.81	2.84 ± 0.60
	11:05	65.72	3.28 ± 0.53
	11:08	65.64	3.64 ± 0.62
	11:49	64.90	3.88 ± 0.57
	11:51	64.88	2.61 ± 0.79
	11:55	64.85	2.27 ± 0.70
	11:57	64.83	3.72 ± 0.60
	16:01	74.87	3.15 ± 0.81
	16:04	75.11	2.32 ± 0.45
	16:16	76.06	3.70 ± 0.72
	16:18	76.23	2.81 ± 0.82
	17:03	80.00	2.61 ± 0.55
	17:06	80.26	3.19 ± 0.39
	17:09	80.52	3.39 ± 0.45
	17:11	80.70	3.54 ± 0.51
Oct. 5	9:08	71.09	3.43 ± 0.43
	9:10	70.95	3.03 ± 0.72
	9:14	70.69	2.91 ± 0.76
	9:16	70.56	2.06 ± 0.81
	10:47	65.90	2.28 ± 0.93
	10:49	65.83	3.35 ± 1.04
	10:52	65.73	2.65 ± 1.16
	10:54	65.66	3.42 ± 1.36
Oct. 6	11:40	64.22	4.85 ± 0.90
	11:42	64.20	3.91 ± 0.55
	11:46	64.15	3.51 ± 0.52
	11:48	64.13	3.43 ± 0.59
	12:49	64.34	3.05 ± 0.71
	12:51	64.37	3.53 ± 0.79
	12:54	64.43	3.49 ± 0.64
	12:57	64.49	2.70 ± 0.79
Oct. 7	10:53	64.91	3.64 ± 0.72
	10:55	64.85	3.94 ± 0.59
	10:59	64.73	3.96 ± 0.64

Table 4-1. (continued)

Date (year, month, day)	Time (45°EMT)	Solar zenith angle (degree)	Vertical column density ($10^{15}cm^{-2}$)
1991 Oct. 7	11:01	64.67	4.73 ± 0.93
	12:02	63.65	3.62 ± 0.76
	12:04	63.65	4.42 ± 0.83
	12:08	63.64	4.28 ± 0.92
	12:10	63.64	3.94 ± 0.83
Oct. 9	9:02	69.95	3.64 ± 0.41
	9:05	69.74	3.56 ± 0.35
	9:08	69.53	3.86 ± 0.55
	9:11	69.33	3.74 ± 0.48
	10:13	65.75	4.45 ± 0.60
	10:16	65.61	3.86 ± 0.55
	10:19	65.47	4.56 ± 0.63
	10:21	65.38	4.58 ± 0.59
	11:04	63.80	5.32 ± 0.53
	11:06	63.80	2.81 ± 0.66
	12:18	62.89	4.10 ± 1.04
	12:21	62.90	4.93 ± 0.82
	13:18	63.88	4.69 ± 0.45
Oct. 10	13:50	64.65	3.52 ± 0.73
	13:52	64.74	3.58 ± 0.95
	13:58	65.00	3.86 ± 1.06
	14:00	65.09	2.84 ± 1.06
Oct. 13	16:56	76.40	5.10 ± 0.39
	16:58	76.58	5.22 ± 0.55
Oct. 15	13:09	61.43	6.56 ± 0.84
	13:12	61.51	5.12 ± 0.57
	13:15	61.70	6.60 ± 0.77
	13:17	61.80	6.76 ± 0.69
Oct. 16	13:37	61.97	5.95 ± 0.62
Nov. 15	14:06	53.88	6.50 ± 1.77
	14:09	54.04	3.36 ± 0.86
	14:12	54.20	5.70 ± 1.06
	14:14	54.31	7.70 ± 2.09
	15:20	58.70	6.22 ± 0.92
	15:23	58.90	5.80 ± 1.29
	15:26	59.08	6.67 ± 0.56
	15:29	59.30	6.19 ± 0.62

Table 4-1. (continued)

Date (year, month, day)	Time (45°EMT)	Solar zenith angle (degree)	Vertical column density ($10^{15}cm^{-2}$)
1991 Nov. 16	13:59	53.26	5.19 ± 0.93
	14:04	53.52	4.60 ± 0.66
	14:09	53.78	4.70 ± 0.94
	14:11	53.89	5.89 ± 0.97
Nov. 20	10:23	51.95	5.54 ± 0.53
	10:26	51.81	5.41 ± 0.88
	14:05	52.59	5.81 ± 1.02
Nov. 22	10:46	50.55	6.64 ± 1.53
	10:50	50.40	7.07 ± 1.20
	10:52	50.30	5.88 ± 1.32
	13:12	49.93	7.28 ± 1.33
	13:15	50.03	6.23 ± 1.60
	13:18	50.12	3.46 ± 1.20
Nov. 25	14:19	52.25	7.21 ± 1.08
	14:21	52.36	7.84 ± 0.81
	14:25	52.60	7.98 ± 1.32
	16:02	59.61	7.07 ± 1.04
	16:04	59.77	5.80 ± 1.25
	16:08	60.10	6.25 ± 1.07
	16:10	60.27	4.25 ± 1.30
Nov. 26	14:07	51.38	6.14 ± 1.76
	14:45	53.63	6.31 ± 0.90
	14:48	53.83	6.45 ± 0.88
Dec. 3	10:34	49.23	8.61 ± 1.27
	10:38	49.05	7.28 ± 1.29
	11:44	47.14	8.33 ± 1.19
	11:46	47.12	8.47 ± 1.02
	11:59	46.99	5.88 ± 1.30
	12:02	46.98	6.42 ± 1.11
Dec. 4	14:55	52.85	5.83 ± 0.77
	14:57	52.99	6.57 ± 0.78
	15:03	53.41	6.08 ± 0.67
	15:59	57.69	5.69 ± 1.06
	16:01	57.86	6.30 ± 1.23
Dec. 14	14:07	48.76	5.59 ± 0.84
	14:09	48.86	6.55 ± 1.39
	14:56	51.67	4.78 ± 1.18

Table 4-1. (continued)

Date (year, month, day)	Time (45°EMT)	Solar zenith angle (degree)	Vertical column density ($10^{15}cm^{-2}$)
1991 Dec. 14	14:59	51.88	5.17 ± 0.99
	15:17	53.15	4.84 ± 0.88
	15:22	53.52	4.57 ± 1.24
	15:25	53.74	4.68 ± 1.55
Dec. 15	12:16	45.76	8.12 ± 2.03
Dec. 16	16:00	56.31	7.21 ± 0.69
	16:06	56.80	4.53 ± 1.01
	16:08	56.97	5.47 ± 0.65
	16:51	60.65	5.35 ± 0.81
	16:53	60.82	5.44 ± 1.13
	16:56	61.09	6.45 ± 1.07
	16:58	61.26	4.40 ± 0.90
Dec. 18	15:12	52.50	5.86 ± 1.12
	15:14	52.60	5.16 ± 1.40
Dec. 21	16:15	57.22	3.68 ± 0.83
	16:17	57.39	5.64 ± 1.26

Table 4-1. (continued)

b. HF

Date (year, month, day)	Time (45°EMT)	Solar zenith angle (degree)	Vertical column density ($10^{15}cm^{-2}$)
1991 Jul. 31	11:53	87.59	0.93 ± 0.16
Aug. 4	13:00	86.52	1.42 ± 0.19
	13:09	86.64	1.42 ± 0.19
	13:12	86.69	1.48 ± 0.19
Aug. 14	12:14	83.50	1.49 ± 0.19
	12:16	83.49	1.45 ± 0.19
Aug. 18	11:13	83.23	1.21 ± 0.18
	11:16	83.15	1.31 ± 0.19
	12:28	82.21	1.09 ± 0.16
	12:31	82.22	1.14 ± 0.16
	10:48	83.04	1.06 ± 0.17
Aug. 21	10:51	82.93	1.12 ± 0.16
	13:10	81.61	1.10 ± 0.17
	13:13	81.67	1.22 ± 0.16
	14:35	84.37	1.28 ± 0.18
	14:38	84.52	1.34 ± 0.18
Aug. 28	11:35	79.30	1.17 ± 0.17
	11:37	79.26	1.29 ± 0.17
	13:06	79.19	1.33 ± 0.18
	13:09	79.24	1.36 ± 0.18
Aug. 29	14:47	82.39	1.42 ± 0.28
	14:50	82.54	1.17 ± 0.21
Aug. 30	9:51	82.49	1.27 ± 0.17
	9:54	82.33	1.54 ± 0.20
Sep. 15	15:25	78.85	1.25 ± 0.17
	15:28	79.05	1.36 ± 0.19
Sep. 16	12:44	71.92	1.28 ± 0.19
	12:46	71.95	1.19 ± 0.19
Sep. 18	10:51	72.50	1.25 ± 0.18
	10:54	72.40	1.20 ± 0.19
Sep. 24	13:54	70.71	1.34 ± 0.22
	13:57	70.83	1.00 ± 0.22
Sep. 29	16:36	79.40	1.59 ± 0.24
	16:42	79.90	1.57 ± 0.24
	16:45	80.15	1.61 ± 0.25
Oct. 3	9:22	70.95	1.26 ± 0.19
	12:47	65.45	1.69 ± 0.25

Table 4-1. (continued)

Date (year, month, day)	Time (45°EMT)	Solar zenith angle (degree)	Vertical column density ($10^{15}cm^{-2}$)
1991 Oct. 3	12:50	65.49	1.56 ± 0.26
Oct. 4	11:37	65.04	1.37 ± 0.23
	11:39	65.01	1.31 ± 0.22
	16:49	78.80	1.88 ± 0.25
	16:51	78.97	1.76 ± 0.23
Oct. 5	9:26	69.91	1.12 ± 0.20
	9:28	69.79	1.24 ± 0.22
Oct. 6	11:59	64.05	1.43 ± 0.23
	12:01	64.04	1.45 ± 0.23
Oct. 7	11:12	64.37	1.32 ± 0.21
	11:14	64.32	1.26 ± 0.22
Oct. 9	9:21	68.68	1.14 ± 0.19
	9:23	68.55	1.30 ± 0.20
Oct. 10	14:14	65.76	1.03 ± 0.17
	14:16	65.86	0.90 ± 0.18
Oct. 13	17:03	77.01	1.00 ± 0.23
	17:05	77.18	1.01 ± 0.20
Nov. 15	14:26	55.00	1.14 ± 0.37
	14:28	55.11	1.11 ± 0.30
Nov. 16	14:17	54.22	1.56 ± 0.29
	14:19	54.33	1.58 ± 0.31
Nov. 20	10:39	51.24	1.34 ± 0.26
	10:41	51.16	1.58 ± 0.28
Nov. 22	10:58	50.12	1.16 ± 0.25
	11:00	50.06	1.22 ± 0.25
Nov. 25	14:37	53.33	1.45 ± 0.26
Nov. 26	16:09	59.98	1.32 ± 0.26
	16:21	60.99	1.31 ± 0.26
Dec. 3	10:46	48.72	1.77 ± 0.41
	10:48	48.64	1.99 ± 0.37
Dec. 4	15:10	53.90	1.46 ± 0.32
	15:12	54.05	1.71 ± 0.31
Dec. 14	14:19	49.40	1.17 ± 0.30
Dec. 16	16:12	57.30	0.79 ± 0.23
	16:14	57.47	1.25 ± 0.27
Dec. 18	15:20	53.05	0.74 ± 0.29
	15:22	53.20	0.68 ± 0.29

Table 4-1. (continued)

c. N_2O

Date (year, month, day)	Time (45°EMT)	Solar zenith angle (degree)	Vertical column density ($10^{18}cm^{-2}$)
1991 Aug. 14	10:59	84.92	6.21 ± 0.58
	11:02	84.83	6.73 ± 0.65
Aug. 18	10:43	84.22	5.77 ± 0.54
	10:44	84.18	5.90 ± 0.55
	13:13	82.63	5.97 ± 0.56
	13:15	82.67	6.48 ± 0.61
Aug. 21	12:23	81.23	6.16 ± 0.57
	12:26	81.23	6.13 ± 0.57
Aug. 25	12:33	79.89	5.73 ± 0.54
Sep. 14	9:54	76.61	5.40 ± 0.51
	9:57	76.45	5.24 ± 0.50
Sep. 15	15:08	77.76	5.99 ± 0.56
	15:11	77.94	6.27 ± 0.58
Sep. 16	12:13	71.78	5.91 ± 0.55
	12:18	71.78	5.81 ± 0.54
Sep. 17	11:02	72.54	6.18 ± 0.58
	11:05	72.45	6.03 ± 0.56
Sep. 18	10:20	73.74	6.02 ± 0.56
	10:22	73.65	5.77 ± 0.54
Sep. 24	13:13	69.39	5.73 ± 0.54
	13:28	69.79	6.19 ± 0.58
	13:29	69.83	5.81 ± 0.54
Sep. 29	10:46	68.30	6.06 ± 0.57
	10:48	68.23	5.79 ± 0.54
Oct. 3	9:00	72.42	5.68 ± 0.53
	9:02	72.28	6.00 ± 0.56
	12:28	65.24	5.94 ± 0.55
	12:30	65.25	5.72 ± 0.54
Oct. 4	11:17	65.42	5.96 ± 0.56
	11:20	65.35	6.17 ± 0.57
	16:28	77.04	6.27 ± 0.58
	16:31	77.29	6.42 ± 0.60
Oct. 5	9:58	68.06	5.78 ± 0.54
	10:01	67.91	5.39 ± 0.50
Oct. 6	12:24	64.06	6.05 ± 0.57
	12:26	64.07	6.30 ± 0.59

Table 4-1. (continued)

Date (year, month, day)	Time (45°EMT)	Solar zenith angle (degree)	Vertical column density ($10^{18}cm^{-2}$)
1991 Oct. 7	11:38	63.86	6.07 ± 0.57
	11:40	63.84	5.91 ± 0.55
Oct. 9	9:49	66.99	5.83 ± 0.54
	9:51	66.88	5.90 ± 0.55
Oct. 13	17:11	77.11	5.87 ± 0.54
	17:13	77.89	5.90 ± 0.55
Nov. 15	14:53	56.71	5.86 ± 0.56
	14:55	56.84	6.14 ± 0.58
Nov. 20	11:14	50.08	5.77 ± 0.55
	11:16	50.03	6.19 ± 0.58
Nov. 22	11:50	49.03	6.30 ± 0.60
	11:56	48.98	6.70 ± 0.63
	11:59	48.97	6.62 ± 0.63
Nov. 25	15:30	57.05	5.93 ± 0.56
	15:35	57.44	5.85 ± 0.56
	15:38	57.67	5.92 ± 0.56
Nov. 26	16:51	63.59	6.35 ± 0.60
	16:54	63.86	6.06 ± 0.57
Dec. 3	11:18	47.66	6.17 ± 0.58
	11:21	47.58	6.38 ± 0.60
Dec. 4	15:30	55.39	5.45 ± 0.52
	15:35	55.77	5.29 ± 0.50
	15:37	55.93	5.31 ± 0.52
Dec. 14	14:30	50.03	6.27 ± 0.59
	14:33	50.20	6.08 ± 0.57
Dec. 16	16:26	58.48	5.76 ± 0.54
	16:29	58.74	5.54 ± 0.52
Dec. 18	15:33	54.02	6.01 ± 0.57
Dec. 21	16:59	61.02	6.14 ± 0.57
	17:02	61.28	6.19 ± 0.59

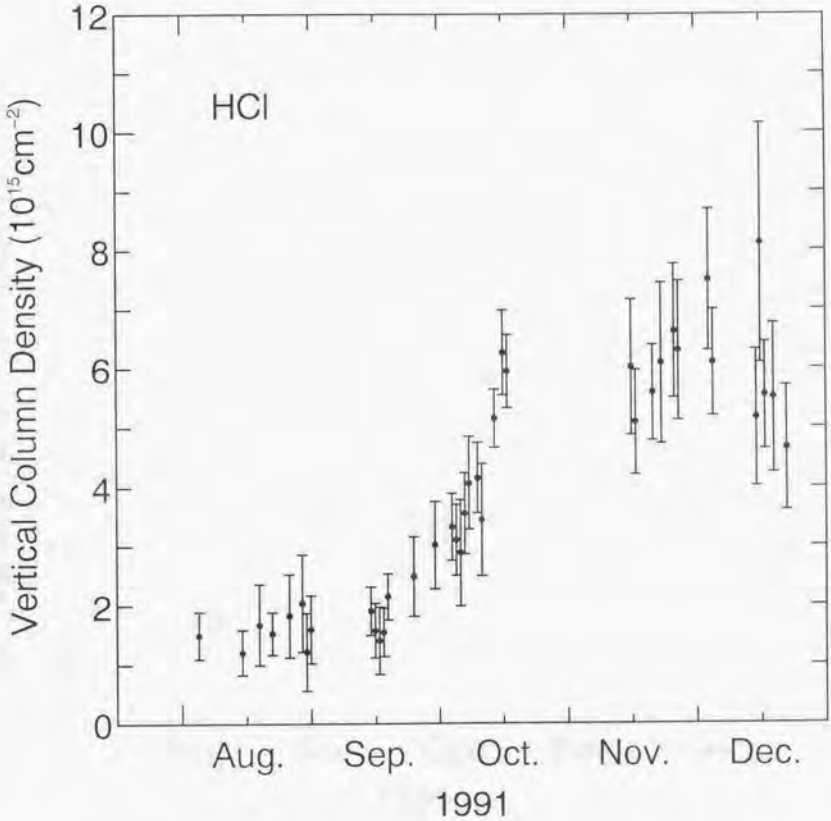

Figure 4-1. Daily averaged HCl vertical column densities at Syowa Station.

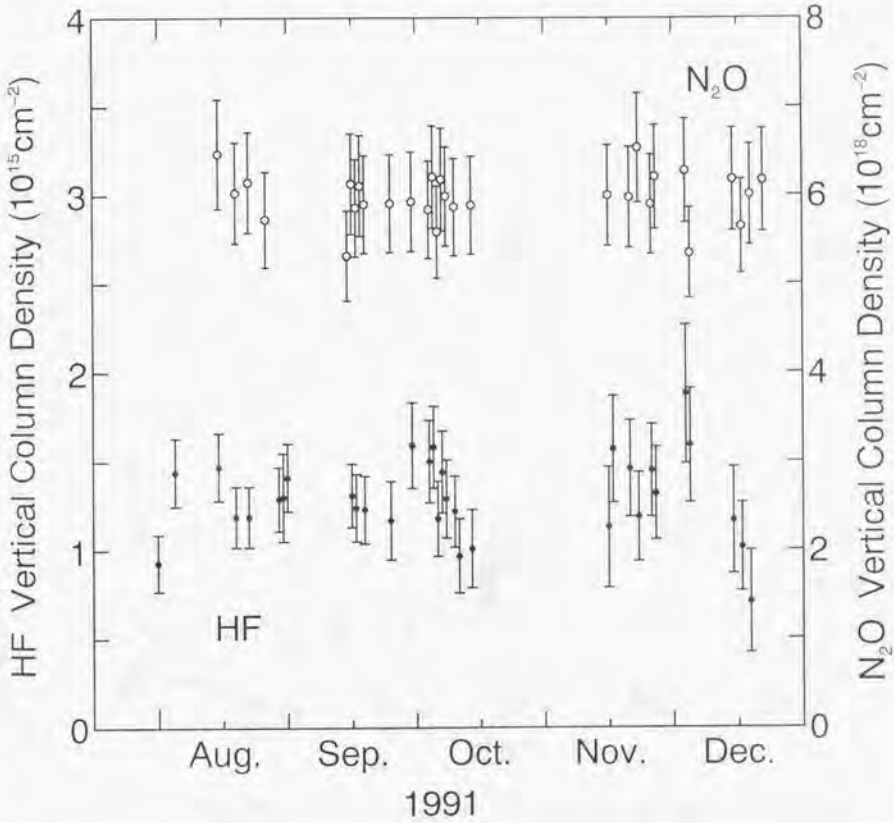

Figure 4-2. Daily averaged HF and N_2O vertical column densities at Syowa Station.

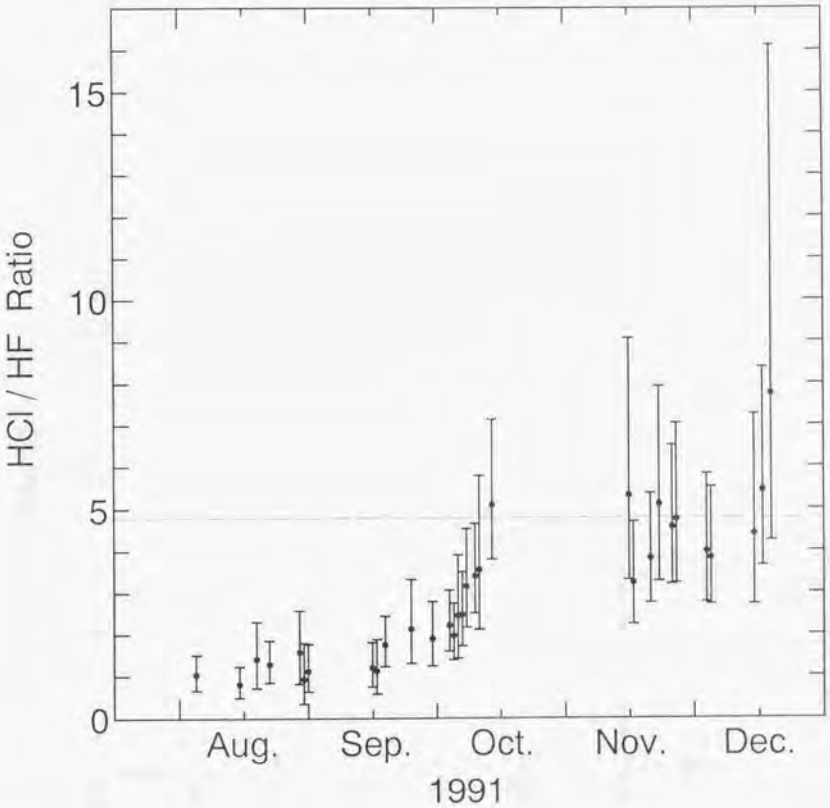

Figure 4-3. HCl/HF vertical column density ratios. Dashed line indicates the average for November and December.

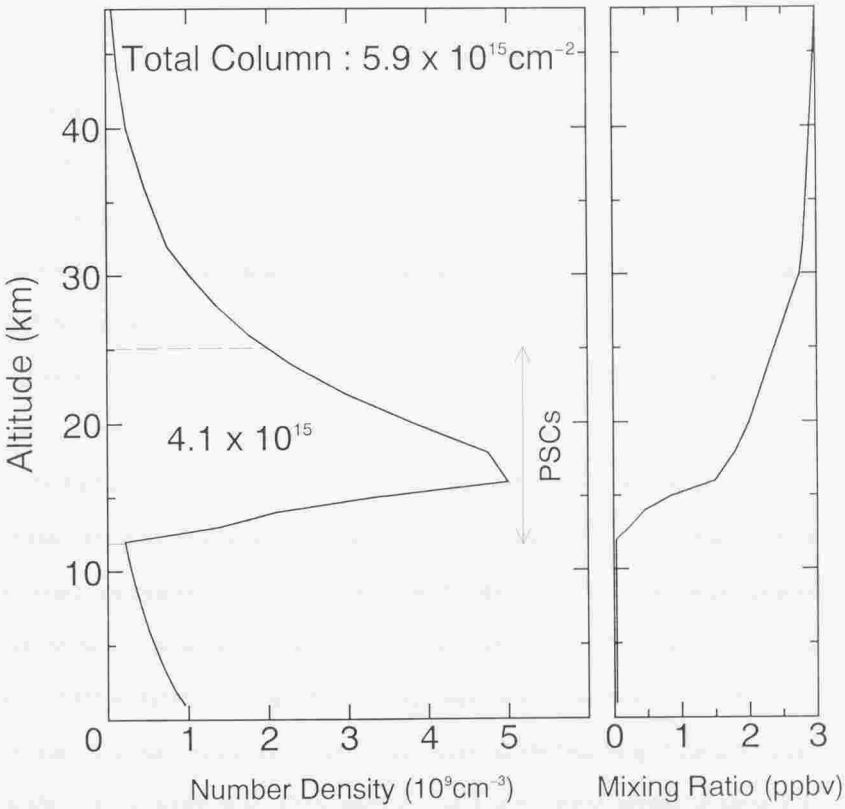

Figure 4-4. Initial HCl number density profile and volume mixing ratio profile for summer.

5 Discussion

The removal of HCl during polar night is considered to occur mainly through the following heterogeneous reactions on PSC particles in the lower stratosphere [Turco *et al.*, 1989; Hanson and Ravishankara, 1991].

$$ClONO_2(g) + HCl(a) \longrightarrow Cl_2(g) + HNO_3(s) \quad (R13)$$
$$N_2O_5(g) + HCl(a) \longrightarrow ClONO(g) + HNO_3(s), \quad (R16)$$

where (g) indicates gas phase, (s) indicates solid crystalline, and (a) indicates surface-adsorbed molecule. One HCl molecule produces one Cl_2 molecule through reaction (R13), and it is photodissociated to produce two Cl atoms which catalytically destroy O_3 after the sunlight come back to polar region. It was concluded from the Arctic measurements of HCl during the second Airborne Arctic Stratospheric Expedition (AASE II) that $ClONO_2$ concentration exceeded HCl concentration at the time of the first PSCs formation and HCl molecules were mostly chemically converted into active chlorine (= Cl + ClO + ClOO + $2\times(ClO)_2$) through reaction (R13) and following photolysis [Webster *et al.*, 1993a, b]. If this case is applicable to the Antarctic stratosphere observed in this study, then a decreased amount of $(4.4\pm1.6) \times 10^{15}cm^{-2}$ in the observed HCl vertical column density corresponds to an amount of active chlorine of $(8.8\pm3.2) \times 10^{15}cm^{-2}$ after the return of sunlight in Antarctic spring. However, gas phase partitioning indicates that the ratio between HCl and $ClONO_2$ in the lower stratosphere at the beginning of the polar night is about 3 : 1 [Kawa *et al.*, 1992], leading to an active chlorine amount of about $3 \times 10^{15}cm^{-2}$.

ClONO molecules produced through reaction (R16) will also be converted into Cl atoms through photodissociation after the return of sunlight in Antarctic spring, but it

may be converted back into the reservoir $ClONO_2$ by the subsequent reactions [Drdla *et al.*, 1993].

$$
\begin{array}{lllllllll}
 & ClONO & + & h\nu & & \longrightarrow & Cl & + & NO_2 & (R31) \\
 & Cl & + & O_3 & & \longrightarrow & ClO & + & O_2 & (R4) \\
 & ClO & + & NO_2 & + \ M & \longrightarrow & ClONO_2 & + & M & (R7) \\
\hline
\text{net:} & ClONO & + & h\nu & + \ O_3 & \longrightarrow & ClONO_2 & + & O_2. & (R32)
\end{array}
$$

One ClONO destroys only one O_3 through these reactions, but if PSCs remain and HCl is available, then the produced $ClONO_2$ may be again converted into active chlorine through reaction (R13) and subsequent photolysis. Furthermore, other heterogeneous reactions such as (R14) and (R15) may be effective in the formation of active chlorine. Some of HCl molecules may be trapped on the surfaces of the PSC particles and may not be converted into active chlorine. These HCl molecules are removed from the stratosphere if sedimentation of the PSC particles occurs. However, we are unable to know which process is effective in the HCl removal with the observation result of this study. The author will discuss how much active chlorine should be produced as a result of these processes using a one-dimensional time-dependent photochemical model for Antarctic spring.

Since the one-dimensional model doesn't include horizontal transport, the dynamical effect in the recovery of HCl must be discussed before using the model. The chemical increase of HCl in the lower stratosphere is determined by the following gas phase reaction

$$Cl + CH_4 \longrightarrow HCl + CH_3. \qquad (R8)$$

This reaction changes active chlorine (Cl) to reservoir (HCl) and occurs simultaneously with the ozone depleting catalytic cycle through ClO dimer ((R18) - (R21)) and the synergetic ClO - BrO catalytic cycle ((R23) - (R26)). However, the reaction rate of (R8) is much smaller than those of the catalytic cycles. Besides this chemical reaction

dynamics may contribute to the recovery of HCl vertical column density. In particular following the movement and destruction of the polar vortex, Syowa Station will be located inside or outside the polar vortex because the latitude of Syowa Station (69°S) is relatively low.

This section will discuss the dynamical effect in the recovery of HCl at first, and next the amount of active chlorine in early spring, finally presenting a scenario for temporal variation of partitioning among chlorine species between 12 and 25 km altitudes from winter to summer in Antarctica.

5.1 Dynamical effect in the recovery of HCl

Figure 5-1 shows temporal variation of daily averaged HCl vertical column densities along with ozone vertical column densities (total ozone) at Syowa Station. Total ozone was measured with a Dobson spectrophotometer by the Japan Meteorological Agency team. Total ozone gradually decreased from August to September and reached minimum of 159 Dobson units (DU) on September 30. Total ozone showed sudden increase and decrease several times from late September to November, and finally reached to a level of about 330 DU in late November through December. The increase in HCl vertical column density began in mid-September while total ozone was decreasing, and was gradual as compared to ozone, implying that the HCl recovery through reaction (R8) occurred simultaneously with ozone depleting catalytic cycles ((R18) - (R21), (R23) - (R26)).

A large and rapid variation in total ozone from late September to November must have been caused by the movement of the polar vortex accompanying the movement of ozone depleted area. Figures 5-2a to 5-2d show examples of the daily maps of total ozone in

southern hemisphere measured by Total Ozone Mapping Spectrometer (TOMS) aboard the Nimbus 7 satellite. On September 30 (Figure 5-2a), a largely ozone-depleted area (so called 'ozone hole') covered the polar region to extend over Syowa Station (indicated by a white dot). It moved away from Syowa Station on October 10 (Figure 5-2b). It became small and slender on November 15 (Figure 5-2c) but covered Syowa Station again, and finally had broken on November 27 (Figure 5-2d). These daily TOMS maps clearly demonstrate that Syowa Station was located inside or sometimes outside the 'ozone hole' from late September to November.

HCl vertical column densities and total ozone at Syowa Station in this period are plotted against the distance from the 'ozone hole' boundary to see the difference of the HCl amount between inside and outside the 'ozone hole' (Figure 5-3). The distance from the 'ozone hole' boundary is defined here as the distance between Syowa Station and the contour line of 275 DU which corresponds to the steepest gradient in total ozone measured with TOMS. The negative values mean Syowa Station is located in the 'ozone hole' and the positive values mean outside. The dashed lines connecting the data points of HCl vertical column densities indicate the sequence of the observation day. Total ozone remains nearly constant with a small value of about 200 DU inside the boundary and gradually increases with an increase of distance outside the boundary. HCl vertical column densities are small inside the boundary and large outside except on November 15 and 16, but the relationship is weak and the change is likely to be due to a temporal development. It should be noteworthy that HCl vertical column densities were as large as the summer level ($(6.07\pm1.20) \times 10^{15}\mathrm{cm}^{-2}$) on November 15 and 16 though the distance from the boundary clearly indicates that Syowa Station was located in the 'ozone hole'

and total ozone was as small as those of September. The small total ozone on November 15 and 16 implies that the air mass over Syowa Station had remained in the 'ozone hole' and had not been subjected to significant mixing of the air mass with that outside the boundary. Therefore, the large HCl vertical column densities observed on November 15 and 16 suggest that HCl had recovered through chemical reactions in the 'ozone hole'. Furthermore it is considered that the removal of HCl molecules by sedimentation of the PSC particles that are trapping HCl molecules are insignificant because HCl vertical column densities of November 15 and 16 are nearly equal to the summer level. This supports recent laboratory measurements suggesting that dechlorination does not result from type II PSC sedimentation [Dominé *et al.*, 1994].

Figure 5-4 shows the temporal variations of atmospheric temperature and wind at 70 hPa level (about 17km altitude) measured with radiosondes by the Japan Meteorological Agency team at Syowa Station. In August and September when Syowa Station was located in the 'ozone hole', atmospheric temperature kept a value of about 190 K low enough to form PSCs, wind direction kept eastward, and wind speed was relatively stable of about 20 m/s. These facts indicate that the dynamical condition of air mass in the 'ozone hole' remained stable in August and September.

It is concluded here that the temporal variation in HCl vertical column density inside the polar vortex from September to November occurred mainly due to chemical reactions, and it is reasonable to assume that the total chlorine amount did not change from winter to summer but that partitioning among chlorine species changed only due to chemical reactions.

5.2 Amount of active chlorine in early spring

A one-dimensional time-dependent photochemical model for Antarctica was used to estimate the amount of active chlorine which gives rise to the observed ozone depletion. The model was modified from that for mid-latitudes developed by Shimazaki and Ogawa [1974]. The model for Antarctica includes 42 chemical species, 108 chemical reactions, and 37 photodissociations. The vertical resolution is 0.5km and extend from the surface to 50 km. The vertical transport of long-lived chemical species and chemical families is represented by vertical eddy diffusion. The principal difference between the models for Antarctica and for mid-latitudes is that the Antarctic model includes the ClO dimer catalytic cycle ((R18) - (R21)). It doesn't include the heterogeneous reactions and the ClO - BrO catalytic cycle ((R23) - (R26)). The simulation was made for the period from the local noon of September 1 to the local noon of October 5, with an integration time step of 120 seconds. The initial vertical distribution of ozone was taken from the ozonesonde measurement on September 3 at Syowa Station carried out by the Japan Meteorological Agency team. The initial vertical distributions of other species were taken from the steady state solution of the model for September 1. However, the vertical distributions of chlorine and nitrogen species were modified to match the assumption that heterogeneous reactions occurred during the polar night. The volume mixing ratios of HCl, $ClONO_2$, NO, NO_2, HNO_3, and N_2O_5 were reduced to 10^{-1} - 10^{-4} of the steady state solution between the altitudes 12 and 25 km where PSCs appear according to observations [e.g., Toon *et al.*, 1989; Coffey *et al.*, 1989], and the volume mixing ratios of Cl, ClO, ClOO, and $(ClO)_2$ were increased to 10 - 10^4 of the steady state solution between the altitudes 12 and 25

km. As for NO_2, the observation at a solar zenith angle of 90° in the same period at Syowa Station show that NO_2 slant column density in September was about one-fourth of that in summer, implying the NO_2 volume mixing ratio in the lower stratosphere was very low (Kondo *et al.*, in press).

The initial values of active chlorine species (Cl, ClO, ClOO, and $(ClO)_2$) were scaled between the altitudes 12 and 25 km in the model calculation in such a way that the calculated ozone depletion might be consistent to the observed depletion. Figure 5-5a shows the best result of the model calculation in which the initial condition for active chlorine distributes between the altitudes 12 and 25 km with $2.9 \times 10^{15}cm^{-2}$ in vertical column density. The calculated total ozone can reconstruct the observed decrease in spring. The calculated HCl increase is also consistent with the observed one if considering that the model doesn't include the heterogeneous reactions. The observed HCl vertical column densities are smaller than the calculated in mid-September. This difference is interpreted with the process that a part of HCl molecules were reconverted into active chlorine through the heterogeneous reactions such as (R13) and (R16) in the presence of PSCs. PSCs appear mainly from June to August, but they often appear in September though they are small in scale [e.g., Collins *et al.*, 1993]. The vertical column density of active chlorine decreases slowly from $2.9 \times 10^{15}cm^{-2}$ on September 1 to $2.1 \times 10^{15}cm^{-2}$ on October 5. The decrease is a consequence of the conversion into reservoir species through the reactions such as (R8).

It is concluded from the results of the model calculations that about $3 \times 10^{15}cm^{-2}$ of active chlorine is required at the beginning of September to explain the observed ozone depletion. Note that the initial value of $2 \times 10^{15}cm^{-2}$ is too small to explain the observed

ozone depletion (Figure 5-5b), but that the initial value of $4 \times 10^{15}cm^{-2}$ is too large (Figure 5-5c). The estimated active chlorine amount of $3 \times 10^{15}cm^{-2}$ may be an uppermost value as the model doesn't include the ClO - BrO catalytic cycle ((R23) - (R26)). If the ClO - BrO catalytic cycle is included, then the additional ozone depletion will occur. Model calculations suggest that ClO - BrO catalytic cycle accounts for about 20 % of the ozone depletion [Jones *et al.*, 1989; Anderson *et al.*, 1989]. Therefore, a smaller amount of active chlorine than $3 \times 10^{15}cm^{-2}$ may be better to explain the ozone depletion. As a result, it can be said that active chlorine of $3 \times 10^{15}cm^{-2}$ or less in vertical column density is required at the beginning of September to explain the observed ozone depletion.

A decrease of $1.5 \times 10^{15}cm^{-2}$ in HCl vertical column density is required to produce $3 \times 10^{15}cm^{-2}$ of active chlorine assuming all active chlorine to be produced through reaction (R13). Even if all active chlorine are converted from HCl, a HCl decrease of $3 \times 10^{15}cm^{-2}$ is enough to produce active chlorine of $3 \times 10^{15}cm^{-2}$. On the other hand, our observation shows that HCl decrease amounts to $(4.4 \pm 1.6) \times 10^{15}cm^{-2}$, about a half of which is converted into active chlorine. The remainder $(1.4 - 2.9) \times 10^{15}cm^{-2}$ should be converted into other chlorine species such as ClONO and/or trapped in the PSC particles.

5.3 Temporal variation of partitioning among chlorine species at lower stratosphere

The results of this study about the partitioning among lower stratospheric chlorine species are summarized as follows:

1. The temporal variations in HCl vertical column density, such as the decrease in winter and the increase from September to November, are determined mostly by

chemical reactions, and little by dynamical effect.

2. The observed decrease of HCl vertical column density in winter amounts to $(4.4 \pm 1.6) \times 10^{15} cm^{-2}$. This means that almost all the HCl molecules in the altitude region between 12 and 25 km are converted into other chlorine species through heterogeneous reactions on the surfaces of the PSC particles and/or trapped on them during the polar night.

3. From the results of the model calculations, active chlorine vertical column density of $3 \times 10^{15} cm^{-2}$ or less is required at the beginning of September to explain the observed ozone depletion.

Figure 5-6 illustrates a scenario proposed for the temporal variation of partitioning among chlorine species between 12 km and 25 km altitudes. In constructing this scenario, there are a few assumptions on the initial condition at the beginning of the polar night. The ratio between HCl and $ClONO_2$ is assumed to be 3 : 1 [Kawa *et al.*, 1992], and chlorine species are assumed to exist in the form of HCl and $ClONO_2$ that are main chlorine reservoirs.

In the presence of PSCs, some HCl and $ClONO_2$ are converted into active chlorine (Cl_2) through the heterogeneous reactions such as (R13). The remainder is converted into less active chlorine such as ClONO and/or trapped in the PSC particles. When the sunshine comes back, Cl_2 molecules are rapidly converted into Cl atoms through photodissociation, and the ozone destroying catalytic cycles ((R18) - (R21), (R23) - (R26)) begin to work. ClONO is converted into Cl and further converted into the reservoir $ClONO_2$ through reactions (R31), (R4), and (R7). At the same time when the catalytic cycles work, the

recovery of HCl through reaction (R8) is slowly going on, and some of $ClONO_2$ are slowly converted into HCl via the following reactions.

$$ClONO_2 + h\nu \longrightarrow Cl + NO_3 \qquad \text{(R33)}$$
$$Cl + CH_4 \longrightarrow HCl + CH_3. \qquad \text{(R8)}$$

All chlorine species are eventually converted into the reservoir HCl and $ClONO_2$ and ozone depletion processes are terminated.

The most important point of this scenario is that all HCl molecules are not converted into active chlorine. However, this is one of possible scenarios and there are still many unknown factors. They are, for example, the amount of $ClONO_2$ at the beginning of the polar night, the amount of HCl trapped on the surfaces of the PSC particles during the polar night, and the amount of total chlorine. No significant dynamical effect inside the polar vortex was observed in this study but other measurements suggest that downwelling had occurred inside the polar vortex [Toon *et al.*, 1989].

To describe the temporal variation of partitioning among chlorine species in detail, we must observe HCl, $ClONO_2$, and ClO simultaneously for at least one year. Furthermore, we should observe other chlorine species and nitrogen species.

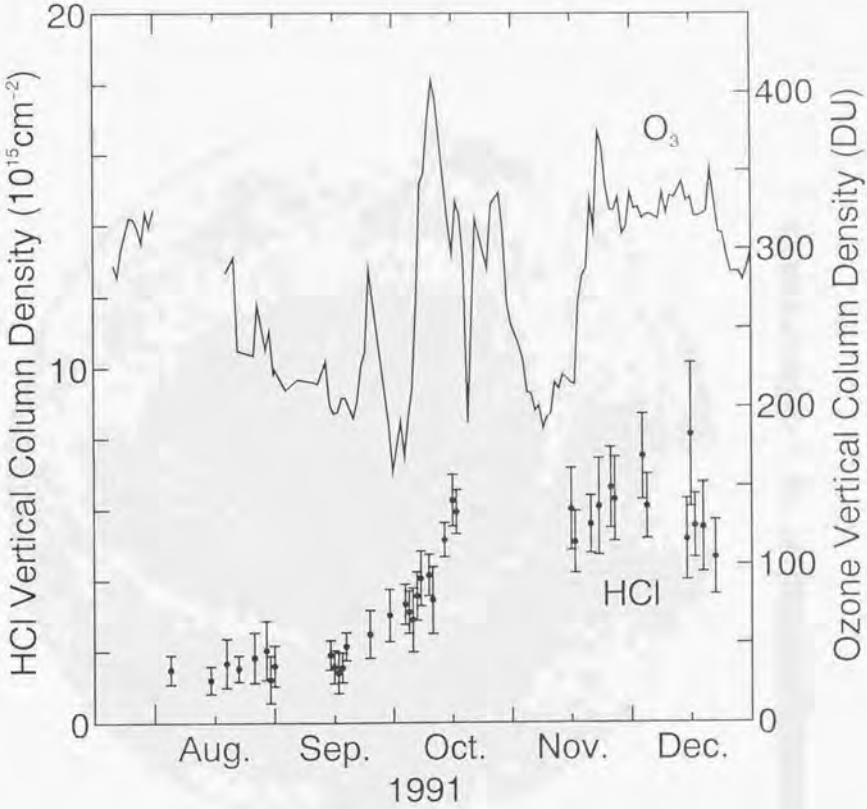

Figure 5-1. Daily averaged HCl vertical column densities with ozone vertical column densities (total ozone) at Syowa Station.

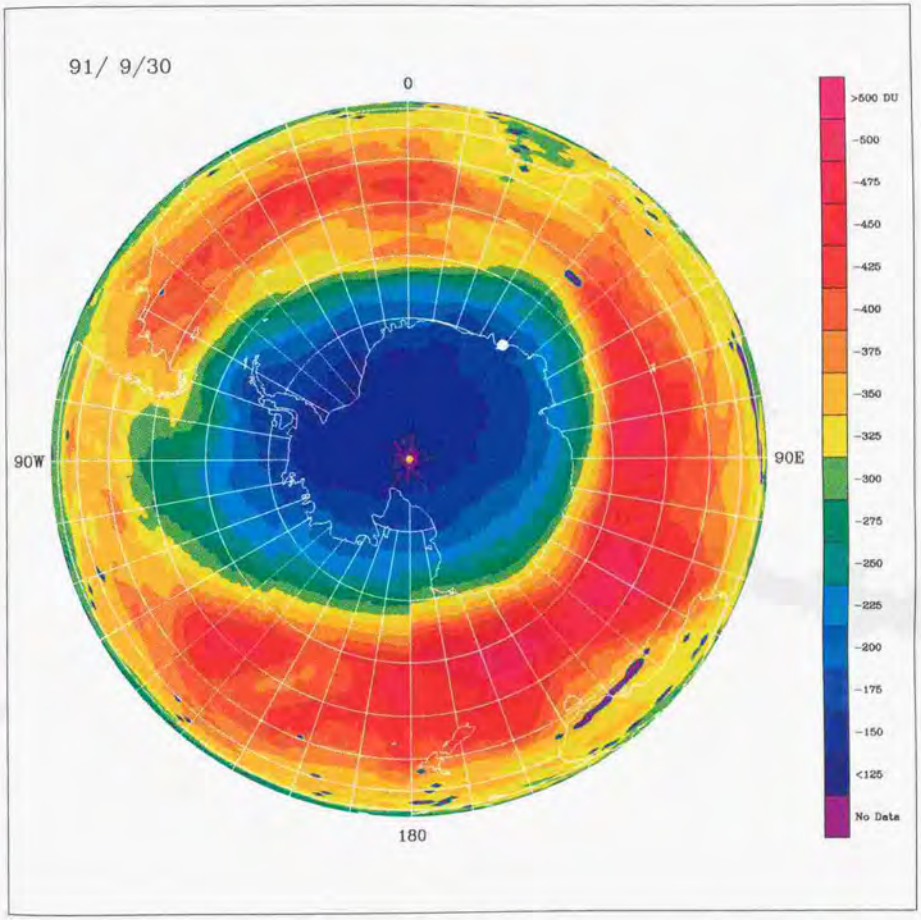

Figure 5-2a. Mapping of total ozone in southern hemisphere on September 30, 1991, measured by Nimbus 7 TOMS. The white dot indicates Syowa Station.

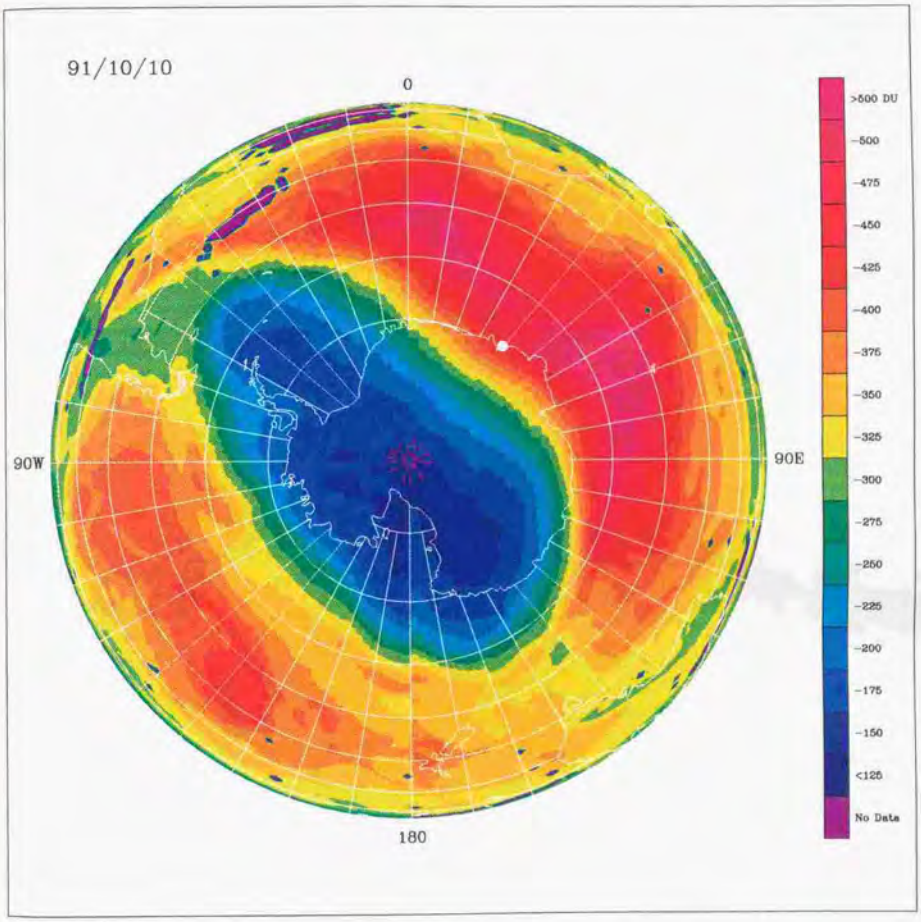

Figure 5-2b. Same as Figure 5-2a, but for October 10, 1991.

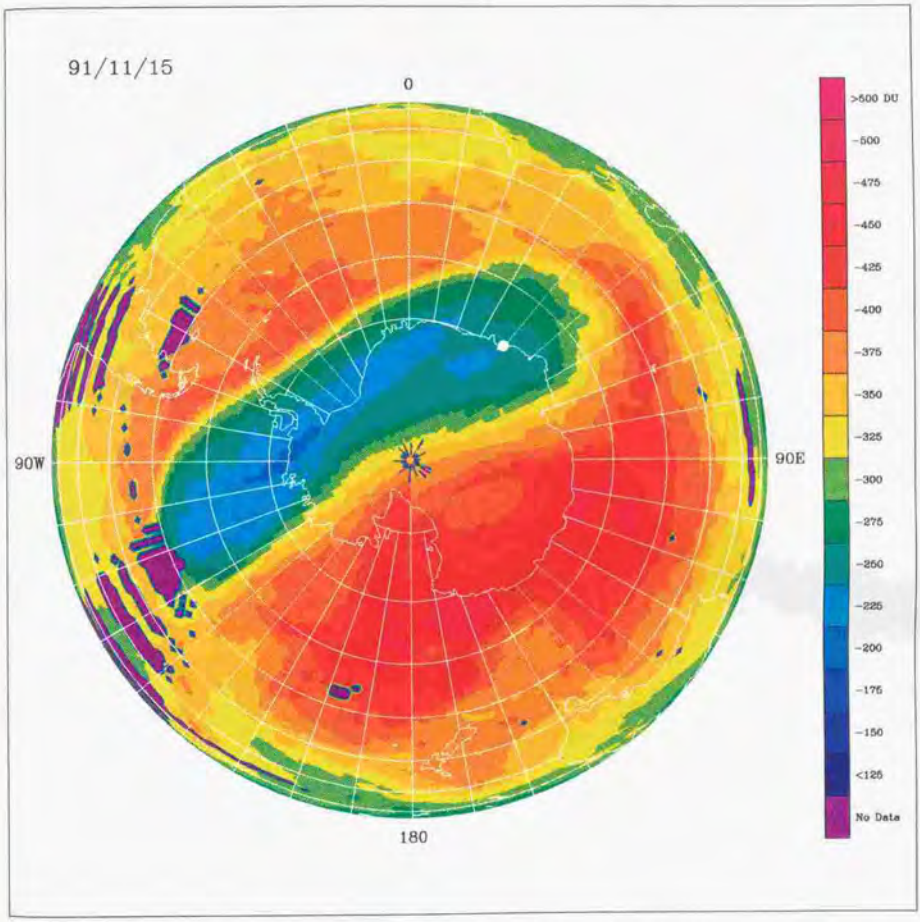

Figure 5-2c. Same as Figure 5-2a, but for November 15, 1991.

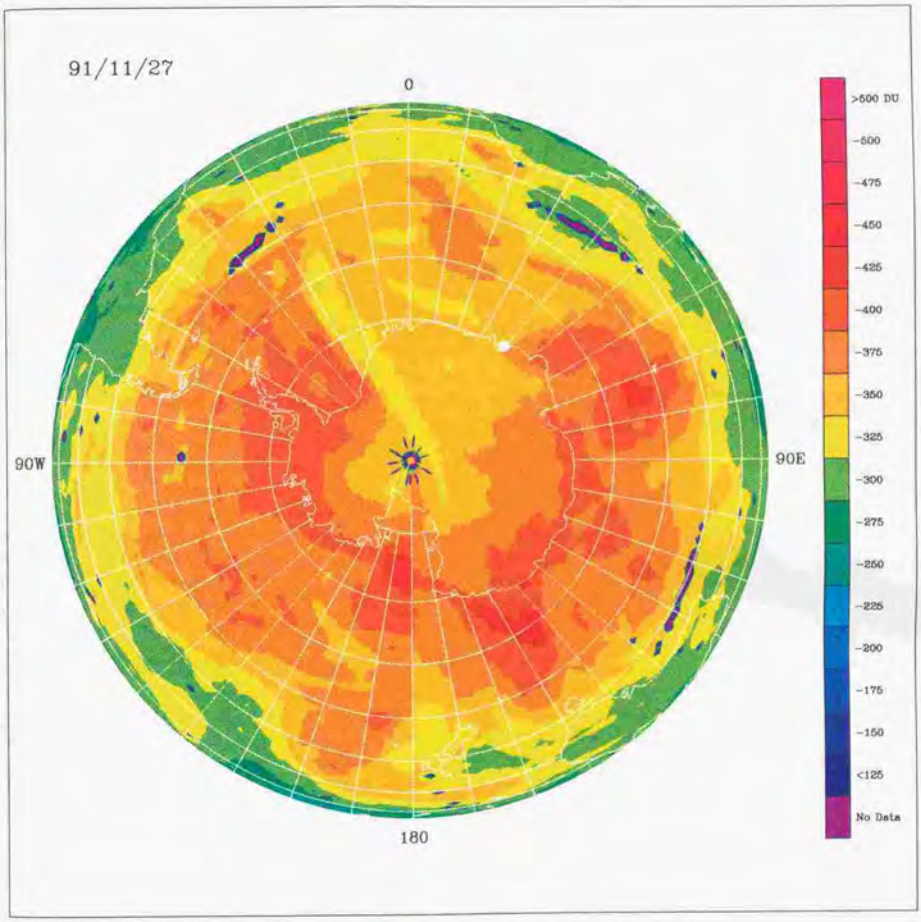

Figure 5-2d. Same as Figure 5-2a, but for November 27, 1991.

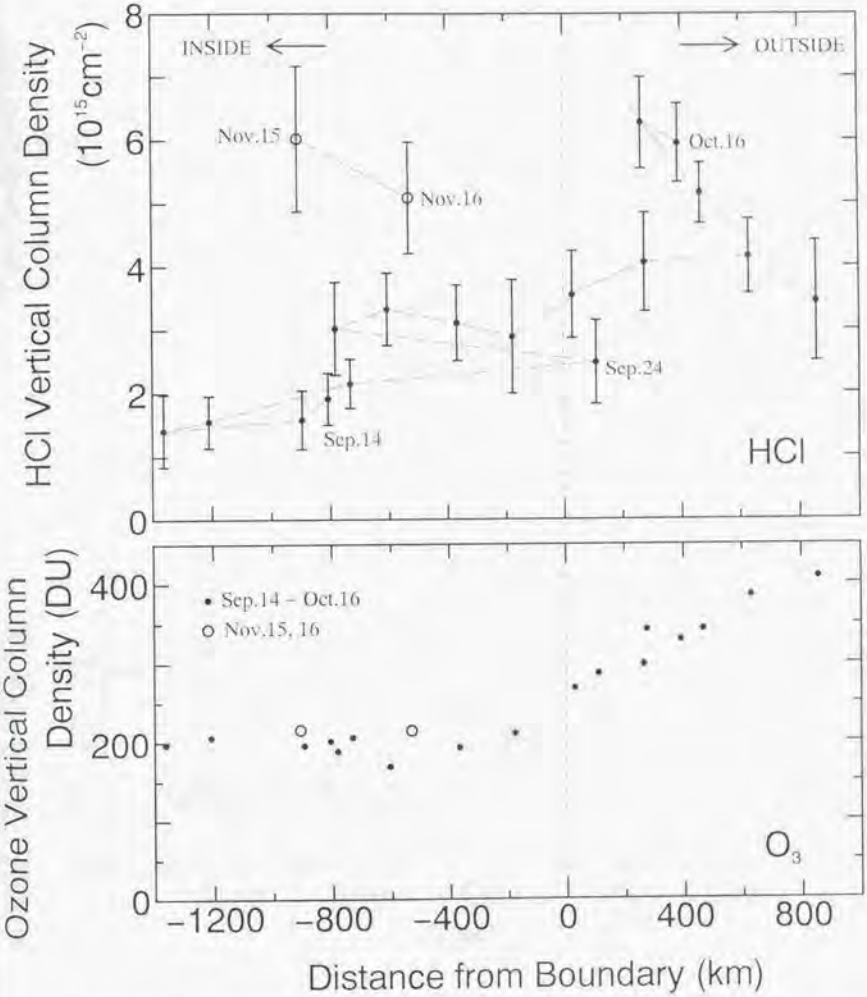

Figure 5-3. HCl and ozone vertical column densities at Syowa Station from September 14 to November 16 versus distance from the 'ozone hole' boundary.

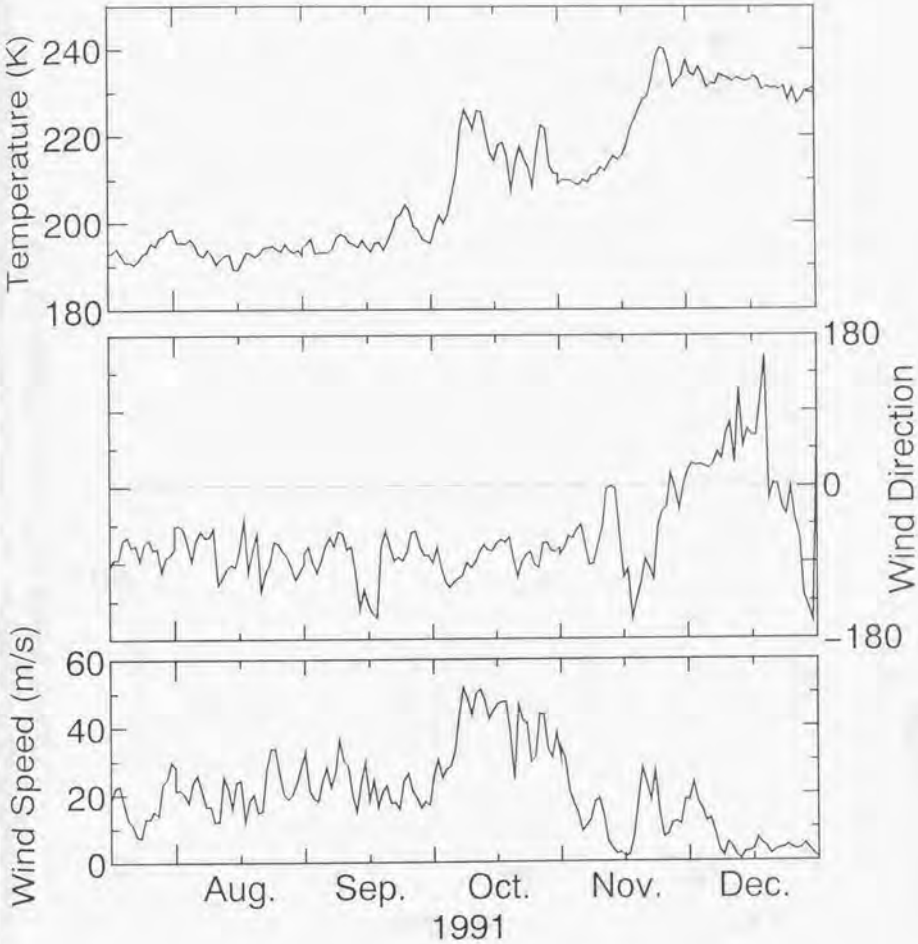

Figure 5-4. Temperature and wind at 70 hPa level at Syowa Station.

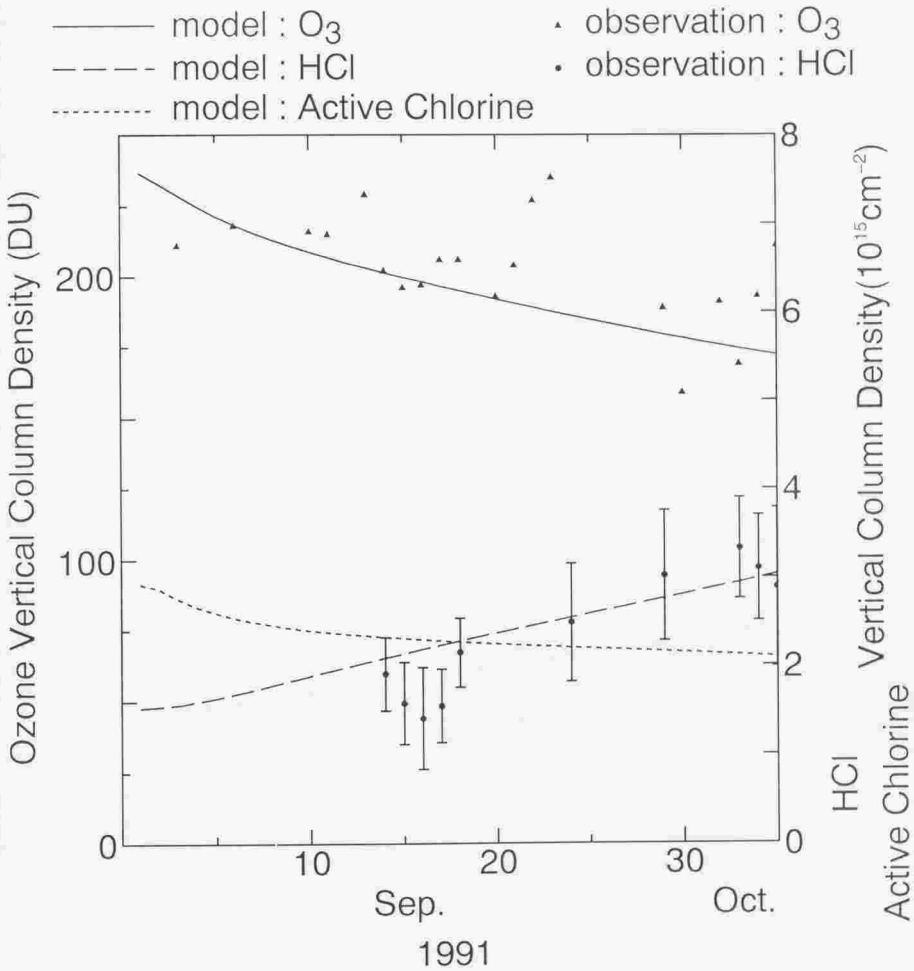

Figure 5-5a. Result of the model calculations with observed ozone and HCl vertical column densities. Initial value of active chlorine vertical column density is $2.9 \times 10^{15}\mathrm{cm}^{-2}$.

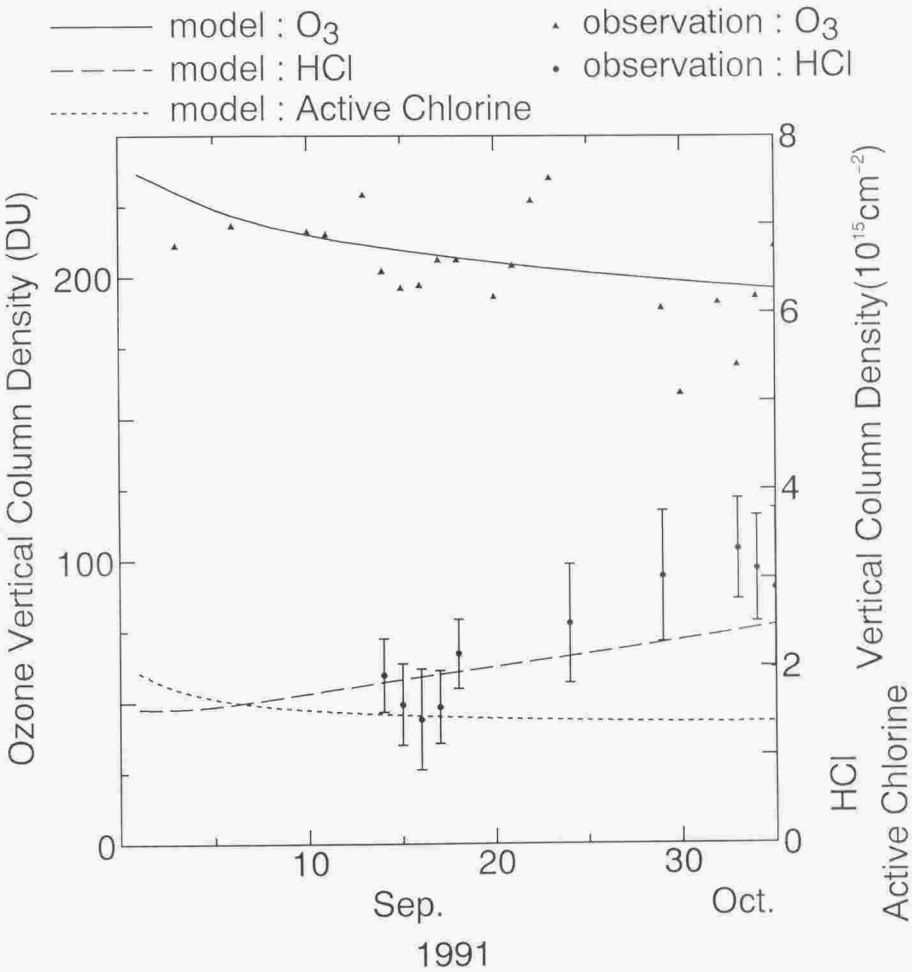

Figure 5-5b. Same as Figure 5-5a, but for initial active chlorine vertical column density of $2.0 \times 10^{15}\mathrm{cm}^{-2}$.

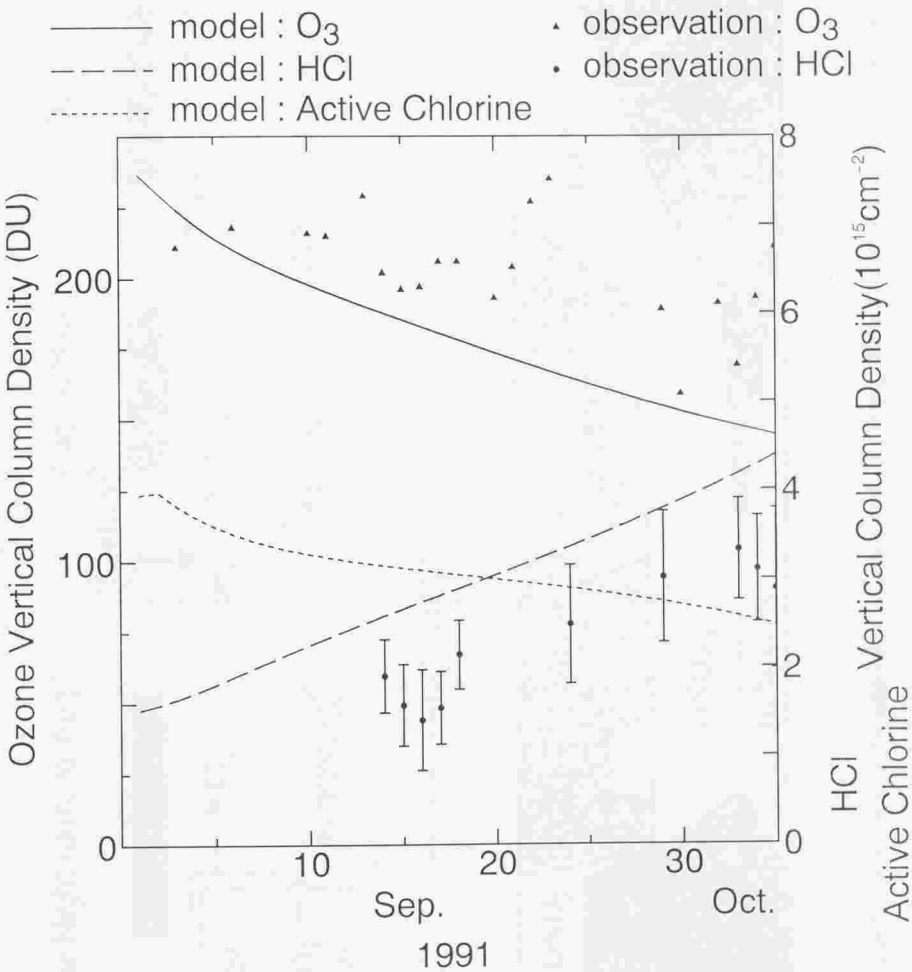

Figure 5-5c. Same as Figure 5-5a, but for initial active chlorine vertical column density of $4.0 \times 10^{15}\mathrm{cm}^{-2}$.

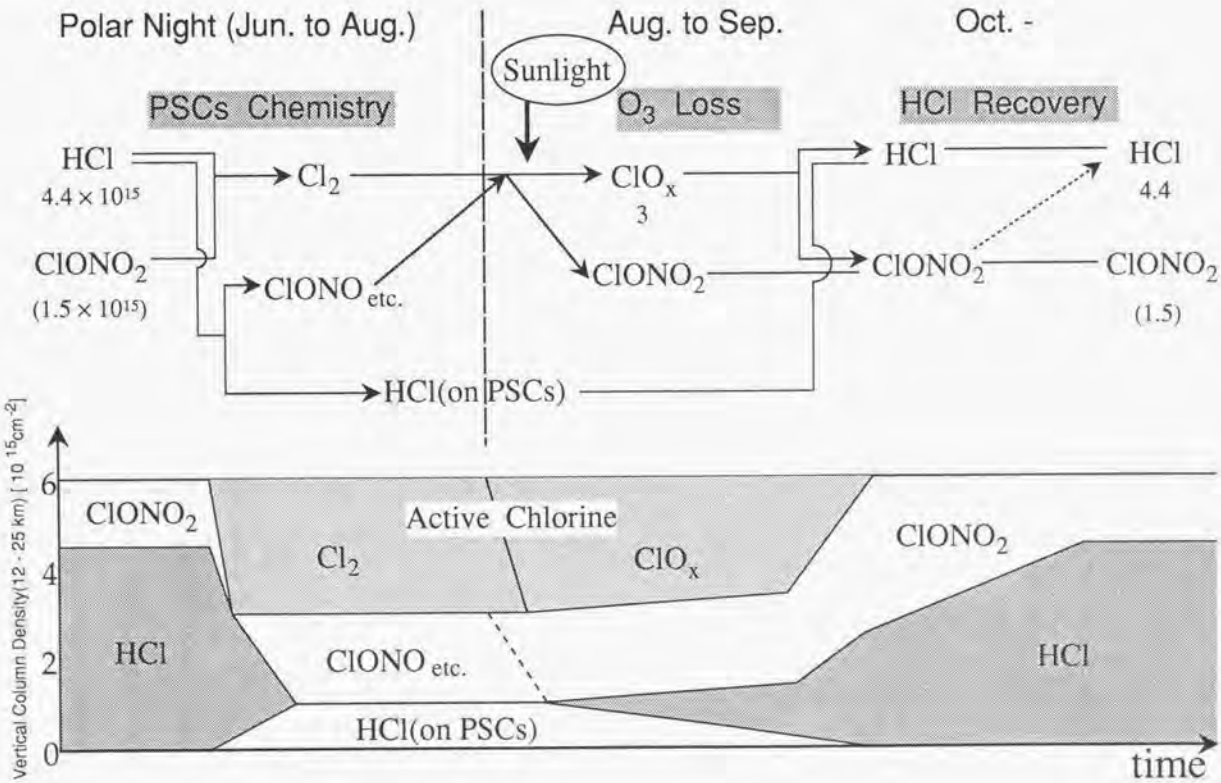

Figure 5-6. A scenario for the temporal variation of partitioning among chlorine species between 12 km and 25 km altitudes.

6 Conclusion

Vertical column densities of HCl, HF and N_2O were observed using solar infrared absorption technique at Syowa Station from July to December 1991, to study the chemistry and dynamics of ozone depletion in the Antarctic stratosphere.

HCl vertical column densities were observed to be $(1.65\pm0.43) \times 10^{15}cm^{-2}$ in winter and to increased to $(6.07\pm1.20) \times 10^{15}cm^{-2}$ in summer. HF and N_2O vertical column densities remained fairly constant at $(1.31\pm0.25) \times 10^{15}cm^{-2}$ and $(5.98\pm0.31) \times 10^{18}cm^{-2}$, respectively from July to December, suggesting stable dynamical conditions. The temporal variation of the HF/HCl vertical column density ratios shows that only HCl was removed by chemical reactions during polar night. These reactions might occur through heterogeneous reactions on the surfaces of the PSC particles in the altitude region between 12km and 25km. The observed HCl removal amount of $(4.4\pm1.6) \times 10^{15}cm^{-2}$ during polar night implies that almost all HCl molecules in this altitude region were converted into other chlorine species and/or trapped in the PSC particles.

Total ozone measured with a Dobson spectrophotometer shows that Syowa Station was located in the 'ozone hole' in mid-November, whereas the HCl vertical column density had recovered to the summer level at that time. Atmospheric temperature and wind over Syowa Station show that the dynamical conditions of air mass in the 'ozone hole' remained stable in August and September. The increase in HCl vertical column density from September to November is thought to be mainly due to chemical reactions. Comparison of the observational result with a one-dimensional time-dependent photochemical model calculation reveals that a half of the decreased amount of HCl vertical column density, (1.5

- 3) $\times$ 10^{15}cm^{-2} was converted into active chlorine, and that the remainder was converted into other less active chlorine species and/or trapped in the PSC particles.

A scenario is proposed for the temporal variation of partitioning among chlorine species between the altitudes 12 and 25 km (Figure 5-6). The most important point of this scenario is that all HCl molecules are not converted into active chlorine. However, to describe the temporal variation of partitioning among chlorine species in detail, we must observe HCl, $ClONO_2$, and ClO simultaneously for longer observation period at least one year. We should observe other chlorine species and nitrogen species.

Acknowledgements

The author would like to thank Prof. T. Ogawa, Prof. N. Iwagami, and Dr. K. Kita for their continuous guidance and encouragement in planning and executing this study. The author also wishes to express his gratitude to all members of the STP group, Department of Earth and Planetary Physics, Graduate School of Science, University of Tokyo.

The monochromator THR1500 was borrowed from the Upper Atmosphere and Space Research Laboratory, Faculty of Science, Tohoku University. The author would like to thank Profs. H. Fukunishi and S. Okano for their generousity. The author also acknowledges valuable comments on setting of the solar-tracker from Prof. K. Shibazaki of Kokugakuin University. The ozone and meteorological data at Syowa Station were provided by the Japan Meteorological Agency.

The observational program was carried out as an activity of the 32nd Japanese Antarctic Research Expedition (JARE-32) that was supported by the National Institute of Polar Research. The author is grateful to Prof. S. Kokubun and all members of JARE-32 for their helpful cooperations.

References

Anderson, J. G., W. H. Brune, S. A. Lloyd, D. W. Toohey, S. P. Sander, W. L. Starr, M. Loewenstein, and J. R. Podolske, Kinetics of O_3 destruction by ClO and BrO within the Antarctic vortex: an analysis based on in situ ER-2 data, *J. Geophys. Res.*, *94*, 11,480-11,520, 1989.

Anderson, J. G., D. W. Toohey, and W. H. Brune, Free radicals within the Antarctic vortex: the role of CFCs in Antarctic ozone loss, *Science*, *251*, 39-46, 1991.

Brasseur, G. and S. Solomon, *Aeronomy of the middle atmosphere*, D. Reidel Publishing Company, Dordrecht, 1986.

Brasseur, G., M. H. Hitchman, S. Walters, M. Dymek, E. Falise, and M. Pirre, An interactive chemical dynamical radiative two-dimensional model of the middle atmosphere, *J. Geophys. Res.*, *95*, 5639-5655, 1990.

Chubachi, S., Relationship between total ozone amounts and stratospheric temperature at Syowa, Antarctica, *J. Geophys. Res.*, *98*, 3005-3010, 1993.

CIRA, COSPAR International Reference Atmosphere, 1972, Berlin, Akademie, 1972.

Coffey, M. T., W. G. Mankin, and A. Goldman, Airborne measurements of stratospheric constituents over Antarctica in the austral spring, 1987 2, Halogen and nitrogen trace gases, *J. Geophys. Res.*, *94*, 16,597-16,613, 1989.

Collins, R. L., K. P. Bowman, C. S. Gardner, Polar stratospheric clouds at the South Pole in 1990: lidar observations and analysis, *J. Geophys. Res.*, *98*, 1001-1010, 1993.

Crutzen, P. J. and U. Schmailzl, Chemical budgets of the stratosphere, *Planet. Space Sci.*, *31*, 1009-1032, 1983.

Deshler, T. and D. J. Hofmann, Ozone profiles at McMurdo Station, Antarctica, the austral spring of 1990, *Geophys. Res. Lett.*, *18*, 657-660, 1991.

de Zafra, R. L., M. Jaramillo, A. Parrish, P. Solomon, B. Connor, and J. Barrett, High concentrations of chlorine monoxide at low altitudes in the Antarctic spring stratosphere: diurnal variation, *Nature*, *328*, 408-411, 1987.

de Zafra, R. L., M. Jaramillo, J. Barrett, L. K. Emmons, P. M. Solomon, and A. Parrish, New observations of a large concentration of ClO in the springtime lower stratosphere over Antarctica and its implications for ozone-depleting chemistry, *J. Geophys. Res.*, *94*, 11,423-11,428, 1989.

Dominé, F., E. Thibert, F. V. Landeghem, E. Silvente, and P. Wagnon, Diffusion and solubility of HCl in ice: preliminary results, *Geophys. Res. Lett.*, *21*, 601-604, 1994.

Drayson, S. R., Rapid computation of the Voigt profile, *J. Quant. Spectrosc. Radiat. Transfer*, *16*, 611-614, 1976.

Drdla, K., R. P. Turco, and S. Elliott, Heterogeneous chemistry on Antarctic polar stratospheric clouds: a microphysical estimate of the extent of chemical processing, *J. Geophys. Res.*, *98*, 8965-8981, 1993.

Eberstein, I. J., Photodissociation of Cl_2O_2 in the spring Antarctic lower stratosphere, *Geophys. Res. Lett.*, *17*, 721-724, 1990.

Elkins, J. W., T. M. Thompson, T. H. Swanson, J. H. butler, B. D. Hall, S. O. Cummings, D. A. Fisher, and A. G. Raffo, Decrease in the growth rates of atmospheric chlorofluorocarbons 11 and 12, *Nature*, *364*, 780-783, 1993.

Elliott, S., R. J. Cicerone, R. P. Turco, K. Drdla, and A. Tabazadeh, Influence of the heterogeneous reaction HCl + HOCl on an ozone hole model with hydrocarbon additions, *J.*

Geophys. Res., *99*, 3497-3508, 1994.

Farman, J. C., B. G. Gardiner, and J. D. Shanklin, Large losses of total ozone in Antarctica reveal seasonal ClO_x/NO_x interaction, *Nature*, *315*, 207-210, 1985.

Farmer, C. B., O. F. Raper, and R. H. Norton, Spectroscopic detection and vertical distribution of HCl in the troposphere and stratosphere, *Geophys. Res. Lett.*, *3*, 13-16, 1976.

Farmer, C. B., G. C. Toon, P. W. Schaper, J.-F. Blavier, and L. L. Lowes, Stratospheric trace gases in the spring 1986 Antarctic atmosphere, *Nature*, *329*, 126-130, 1987.

Farmer, C. B., B. Carli, A. Bonetti, M. Carlotti, B. M. Dinelli, H. Fast, W. F. J. Evans, N. Louisnard, C. Alamichel, W. Mankin, M. Coffey, I. G. Nolt, D. G. Murcray, A. Goldman, G. M. Stokes, D. W. Johnson, W. A. Traub, K. V. Chance, R. Zander, G. Roland, and L. Delbouille, Balloon Intercomparison Campaigns: results of remote sensing measurements of HCl, *J. Atmos. Chem.*, *10*, 237-272, 1990.

Girard, A., G. Fergant, L. Gramont, O. L. -Bordowsky, J. Laurent, S. Le Boiteux, M. P. Lemaitre, and N. Louisnard, Latitudinal distribution of ten stratospheric species deduced from simultaneous spectroscopic measurements, *J. Geophys. Res.*, *88*, 5377-5392, 1983.

Gleason, J. F., P. K. Bhartia, J. R. Herman, R. McPeters, P. Newman, R. S. Stolarski, L. Flynn, G. Labow, D. Larko, C. Seftor, C. Wellemeyer, W. D. Komhyr, A. J. Miller, and W. Planet, Record low global ozone in 1992, *Science*, *260*, 523-526, 1993.

Goldman, A., F. J. Murcray, F. H. Murcray, and D. G. Murcray, Quantification of HCl from high resolution infrared spectra obtained at the South Pole in December 1986, *Geophys. Res. Lett.*, *14*, 622-623, 1987.

Granier, C. and G. Brasseur, Impact of heterogeneous chemistry on model predictions of

ozone changes. *J. Geophys. Res.*, *97*, 18,015-18,033, 1992.

Hanson, D. R. and A. R. Ravishankara, The reaction probabilities of $ClONO_2$ and N_2O_5 on polar stratospheric cloud materials, *J. Geophys. Res.*, *96*, 5081-5090, 1991.

Henderson, G. S., W. F. J. Evans, and J. C. McConnell, Effects of initial active chlorine concentrations on the Antarctic ozone spring depletion, *J. Geophys. Res.*, *95*, 1899-1908, 1990.

Herman, J. R., R. McPeters, and D. Larko, Ozone depletion at northern and southern latitudes derived from January 1979 to December 1991 Total Ozone Mapping Spectrometer data, *J. Geophys. Res.*, *98*, 12,783-12,793, 1993.

Hills, A. J., R. J. Cicerone, J. G. Calvert, and J. W. Birks, Kinetics of the BrO + ClO reaction and implications for stratospheric ozone, *Nature*, *328*, 405-408, 1987.

Hofmann, D. J., S. J. Oltmans, J. A. Lathrop, J. M. Harris, and H. Vömel, Record low ozone at the South Pole in the spring of 1993, *Geophys. Res. Lett.*, *21*, 421-424, 1994.

Jackman, C. H., J. E. Nielsen, D. J. Allen, M. C. Cerniglia, R. D. McPeters, A. R. Douglass, and R. B. Rood, The effects of the October 1989 solar proton events on the stratosphere as computed using a three-dimensional model, *Geophys. Res. Lett.*, *20*, 459-462, 1993.

Jones, R. L., J. Austin, D. S. McKenna, J. G. Anderson, D. W. Fahey, C. B. Farmer, L. E. Heidt, K. K. Kelly, D. M. Murphy, M. H. Proffitt, A. F. Tuck, and J. F. Vedder, Lagrangian photochemical modeling studies of the 1987 Antarctic spring vortex 1. Comparison with AAOE observations, *J. Geophys. Res.*, *94*, 11,529-11,558, 1989.

Kawa, S. R., D. W. Fahey, L. E. Heidt, W. H. Pollock, S. Solomon, D. E. Anderson, M. Loewenstein, M. H. Proffitt, J. J. Margitan, and K. R. Chan, Photochemical partitioning of the reactive nitrogen and chlorine reservoirs in the high-latitude stratosphere, *J.*

Geophys. Res., *97*, 7905-7923, 1992.

Kaye, J. A., A. R. Douglass, C. H. Jackman, R. S. Stolarski, R. Zander, and G. Roland, Two-dimensional model calculation of fluorine-containing reservoir species in the stratosphere, *J. Geophys. Res.*, *96*, 12,865-12,881, 1991.

Keys, J. G. and B. G. Gardiner, NO_2 overnight decay and layer height at Halley Bay, Antarctica, *Geophys. Res. Lett.*, *18*, 665-668, 1991.

Koehler, B. G., L. S. McNeill, A. M. Middlebrook, and M. A. Tolbert, Fourier transform infrared studies of the interaction of HCl with model polar stratospheric cloud films, *J. Geophys. Res.*, *98*, 10,563-10,571, 1993.

Koike, M., Y. Kondo, M. Hayashi, Y. Iwasaka, P. A. Newman, M. Helten, and P. Aimedieu, Depletion of Arctic ozone in the winter 1990, *Geophys. Res. Lett.*, *18*, 791-794, 1991.

Kondo, Y., W. A. Matthews, S. Solomon, M. Hayashi, M. Koike, K. Yamazaki, H. Nakajima, and K. Tsukui, Ground based measurements of column amounts of NO_2 over Syowa Station, Antarctica, *J. Geophys. Res.*, in press.

Liu, X., R. D. Blatherwick, F. J. Murcray, J. G. Keys, and S. Solomon, Measurements and model calculations of HCl column amounts and related parameters over McMurdo during the austral spring in 1989, *J. Geophys. Res.*, *97*, 20,795-20,804, 1992.

Mankin, W. G. and M. T. Coffey, Latitudinal distributions and temporal changes of stratospheric HCl and HF, *J. Geophys. Res.*, *88*, 10,776-10,784, 1983.

Mankin, W. G. and M. T. Coffey, Increased stratospheric hydrogen chloride in the El Chichón cloud, *Science*, *226*, 170-172, 1984.

Mankin, W. G., M. T. Coffey, K. V. Chance, W. A. Traub, B. Carli, F. Mencaraglia, S. Piccioli, I. G. Nolt, J. V. Radostitz, S. Zander, G. Roland, D. W. Johnson, G. M. Stokes,

C. B. Farmer, and R. K. Seals, Intercomparison of measurements of stratospheric hydrogen fluoride, *J. Atmos. Chem.*, *10*, 219-236, 1990.

Mankin, W. G., M. T. Coffey, and A. Goldman, Airborne observations of SO_2, HCl, and O_3, in the stratospheric plume of the Pinatubo volcano in July 1991, *Geophys. Res. Lett.*, *19*, 179-182, 1992.

Marché, P., A. Barbe, C. Secroun, J. Corr, and P. Jouve, Ground based spectroscopic measurements of HCl, *Geophys. Res. Lett.*, *7*, 869-872, 1980.

McElroy, M. B., R. J. Salawitch, S. C. Wofsy, and J. A. Logan, Reductions of Antarctic ozone due to synergistic interactions of chlorine and bromine, *Nature*, *321*, 759-762, 1986.

McElroy, M. B., R. J. Salawitch, and S. C. Wofsy, Chemistry of the Antarctic stratosphere, *Planet. Space Sci.*, *36*, 73-87, 1988.

Müller, R. and P. J. Crutzen, A possible role of galactic cosmic rays in chlorine activation during polar night, *J. Geophys. Res.*, *98*, 20,483-20,490, 1993.

Makino, Y., H. Muramatsu, S. Kawaguchi, T. Yamanouchi, M. Tanaka, and T. Ogawa, Spectroscopic measurements of atmospheric N_2O at Syowa Station, Antarctica (abstract), *Mem. Natl. Inst. Polar Res., Spec. Issue*, *45*, 93-94, 1986.

Muramatsu, H., Y. Makino, M. Hirota, and T. Sasaki, Infrared measurements of total nitrous oxide at Tsukuba, *Mem. Natl. Inst. Polar Res., Spec. Issue*, *34*, 28-36, 1984.

Murcray, F. J., A. Goldman, R. Blatherwick, A. Matthews, and N. Jones, HNO_3 and HCl amounts over McMurdo during the spring of 1987, *J. Geophys. Res.*, *94*, 16,615-16,618, 1989.

Notholt, J., R. Neuber, O. Schrems, and T. V. Clarmann, Stratospheric trace gas concentrations in the Arctic polar night derived by FTIR-spectroscopy with the moon as IR light

source, *Geophys. Res. Lett.*, *20*, 2059-2062, 1993.

Pommereau, J. P. and U. Schmidt, CHEOPS III: An ozone research campaign in the Arctic winter stratosphere 1989/90, *Geophys. Res. Lett.*, *18*, 759-762, 1991.

Prasad, S. S., Electron scavenging of stratospheric chlorine to reduce ozone depletion: will it work?, *J. Geophys. Res.*, *98*, 18,597-18,598, 1993.

Proffitt, M. H., J. A. Powell, A. F. Tuck, D. W. Fahey, K. K. Kelly, A. J. Krueger, M. R. Schoeberl, B. L. Gary, J. J. Margitan, K. R. Chan, M. Loewenstein, and J. R. Podolske, A chemical definition of the boundary of the Antarctic ozone hole, *J. Geophys. Res.*, *94*, 11,437-11,448, 1989.

Reid, G. C., S. Solomon, R. R. Garcia, Response of the middle atmosphere to the solar proton events of August-December, 1989, *Geophys. Res. Lett.*, *18*, 1019-1022, 1991.

Rinsland, C. P., A. Goldman, F. J. Murcray, D. G. Murcray, M. A. H. Smith, R. K. Seals, Jr., J. C. Larsen, and P. L. Rinsland, Stratospheric N_2O mixing ratio profile from high-resolution balloon-borne solar absorption spectra and laboratory spectra near 1880 cm^{-1}, *Appl. Opt.*, *21*, 4351-4355, 1982.

Rinsland, C. P., J. S. Levine, A. Goldman, N. D. Sze, M. K. W. Ko, and D. W. Johnson, Infrared measurements of HF and HCl total column abundances above Kitt Peak, 1977-1990 : Seasonal cycles, long-term increases, and comparisons with model calculations, *J. Geophys. Res.*, *96*, 15,523-15,540, 1991.

Rodriguez, J. M., M. K. W. Ko, N. D. Sze, S. D. Pierce, J. G. Anderson, D. W. Fahey, K. Kelly, C. B. Farmer, G. C. Toon, M. T. Coffey, L. E. Heidt, W. G. Mankin, K. R. Chan, W. L. Starr, J. F. Vedder, and M. P. McCormick, Nitrogen and chlorine species in the spring Antarctic stratosphere: comparison of models with Airborne Antarctic Ozone

Experiment observations. *J. Geophys. Res.*, *94*, 16,683-16,703, 1989.

Rood, R. B., J. E. Nielsen, R. S. Stolarski, A. R. Douglass, J. A. Kaye, and D. J. Allen, Episodic total ozone minima and associated effects on heterogeneous chemistry and lower stratospheric transport, *J. Geophys. Res.*, *97*, 7979-7996, 1992.

Rothman, L. S., R. R. Gamache, R. H. Tipping, C. P. Rinsland, M. A. H. Smith, D. C. Benner, V. M. Devi, J. -M. Flaud, C. C. -Peyret, A. Perrin, A. Goldman, S. T. Massie, L. R. Brown, and R. A. Toth, The HITRAN molecular database: editions of 1991 and 1992, *J. Quant. Spectrosc. Radiat. Transfer*, *48*, 469-507, 1992.

Russell, J. M., III, A. F. Tuck, L. L. Gordley, J. H. Park, S. R. Drayson, J. E. Harries, R. J. Cicerone, and P. J. Crutzen, HALOE Antarctic observations in the spring of 1991, *Geophys. Res. Lett.*, *20*, 719-722, 1993.

Russell, J. M., III, L. L. Gordley, J. H. Park, S. R. Drayson, W. D. Hesketh, R. J. Cicerone, A. F. Tuck, J. E. Frederick, J. E. Harries, and P. J. Crutzen, The halogen occultation experiment, *J. Geophys. Res.*, *98*, 10,777-10,797, 1993.

Sanders, R. W., S. Solomon, J. P. Smith, L. Perliski, H. L. Miller, G. H. Mount, J. G. Keys, and A. L. Schmeltekopf, Visible and near-ultraviolet spectroscopy at McMurdo Station, Antarctica 9. Observations of OClO from April to October 1991, *J. Geophys. Res.*, *98*, 7219-7228, 1993.

Shimazaki, T. and T. Ogawa, On the theoretical model of vertical distributions of minor neutral constituents concentrations in the stratosphere, *Tech. Memo. ERL-OD 20*, NOAA, Boulder, Colo., 1974.

Solomon, S., R. R. Garcia, F. S. Rowland, and D. J. Wuebbles, On the depletion of Antarctic ozone, *Nature*, *321*, 755-758, 1986.

Solomon, S., The mystery of the Antarctic ozone "hole", *Rev. Geophys.*, *26*, 131-148, 1988.

Solomon, S., Progress towards a quantitative understanding of Antarctic ozone depletion, *Nature*, *347*, 347-354, 1990.

Solomon, S. and J. G. Keys, Seasonal variations in Antarctic NO_x chemistry, *J. Geophys. Res.*, *97*, 7971-7978, 1992.

Solomon, S., J. P. Smith, R. W. Sanders, L. Perliski, H. L. Miller, G. H. Mount, J. G. Keys, and A. L. Schmeltekopf, Visible and near-ultraviolet spectroscopy at McMurdo Station, Antarctica 8. Observations of Nighttime NO_2 and NO_3 from April to October 1991, *J. Geophys. Res.*, *98*, 993-1000, 1993.

Strahan, S. E., M. Loewenstein, J. R. Podolske, W. L. Starr, K. R. Chan, M. H. Proffitt, and K. K. Kelly, Correlation of N_2O and ozone in the southern polar vortex during the Airborne Antarctic Ozone Experiment, *J. Geophys. Res.*, *94*, 16,749-16,756, 1989.

Symonds, R. B., W. I. Rose, and M. H. Reed, Contribution of Cl- and F-bearing gases to the atmosphere by volcanoes, *Nature*, *334*, 415-418, 1988.

Toon, G. C., C. B. Farmer, L. L. Lowes, P. W. Schaper, J.-F. Blavier, and R. H. Norton, Infrared aircraft measurements of stratospheric composition over Antarctica during September 1987, *J. Geophys. Res.*, *94*, 16,571-16,596, 1989.

Toon, G. C., C. B. Farmer, P. W. Schaper, L. L. Lowes, and R. H. Norton, Composition Measurements of the 1989 Arctic winter stratosphere by airborne infrared solar absorption spectroscopy, *J. Geophys. Res.*, *97*, 7939-7961, 1992.

Toon, G. C., J.-F. Blavier, J. N. Solario, and J. T. Szeto, Airborne observations of the of the composition of the 1992 tropical stratosphere by FTIR solar absorption spectrometry, *Geophys. Res. Lett.*, *20*, 2503-2506, 1993.

Toumi, R., R. L. Jones, and J. A. Pyle, Stratospheric ozone depletion by $ClONO_2$ photolysis, *Nature*, *365*, 37-39, 1993.

Turco, R. P., O. B. Toon, and P. Hamill, Heterogeneous physicochemistry of the polar ozone hole, *J. Geophys. Res.*, *94*, 16,493-16,510, 1989.

Wahner, A. R. O. Jakoubek, G. H. Mount, A. R. Ravishankara, and A. L. Schmeltekopf, Remote sensing observations of nighttime OClO column during the Airborne Antarctic Ozone Experiment, September 8, 1987, *J. Geophys. Res.*, *94*, 11,405-11,411, 1989.

Wahner, A. and C. Schiller, Twilight variation of vertical column abundances of OClO and BrO in north polar region, *J. Geophys. Res.*, *97*, 8047-8055, 1992.

Wallace, L. and W. Livingston, Spectroscopic observations of atmospheric trace gases over Kitt Peak 3. Long-term trends of hydrogen chloride and hydrogen fluoride from 1978-1990, *J. Geophys. Res.*, *96*, 15,513-15,521, 1991.

Wallace, L. and W. Livingston, The effect of the Pinatubo cloud on hydrogen chloride and hydrogen fluoride, *Geophys. Res. Lett.*, *19*, 1209, 1992.

Warneck, P., *Chemistry of the natural atmosphere*, Academic Press Inc., San Diego, 1988.

Waters, J. W., L. Froidevaux, W. G. Read, G. L. Manney, L. S. Elson, D. A. Flower, R. F. Jarnot, and R. S. Harwood, Stratospheric ClO and ozone from the microwave limb sounder on the Upper Atmosphere Research Satellite, *Nature*, *362*, 597-602, 1993.

Webster, C. R., R. D. May, D. W. Toohey, L. M. Avallone, J. G. Anderson, P. Newman, L. Lait, M. R. Schoeberl, J. W. Elkins, and K. R. Chan, Chlorine chemistry on polar stratospheric cloud particles in the Arctic winter, *Science*, *261*, 1130-1134, 1993a.

Webster, C. R., R. D. May, D. W. Toohey, L. M. Avallone, J. G. Anderson, and S. Solomon, In situ measurements of the ClO/HCl ratio: heterogeneous processing on sulfate aerosols

and polar stratospheric clouds. *Geophys. Res. Lett.*, *20*, 2523-2526, 1993b.

Wofsy, S. C., M. J. Molina, R. J. Salawitch, L. E. Fox, and M. B. McElroy, Interactions between HCl, NO_x, and H_2O ice in the Antarctic stratosphere: implications for ozone, *J. Geophys. Res.*, *93*, 2442-2450, 1988.

World Meteorological Organization, Atmospheric ozone 1985 – Assessment of our understanding of the processes controlling its present distribution and change, *Rep. 16*, 1986.

World Meteorological Organization/United Nations Environment Program, Scientific assessment of ozone depletion: 1991, *Rep. 25*, 1992.

World Meteorological Organization/United Nations Environment Program, Radiative forcing of climate, 1994.

Zander, R., G. Roland, L. Delbouille, A. Sauval, C. B. Farmer, and R. H. Norton, Monitoring of the integrated column of hydrogen fluoride above the Jungfraujoch Station since 1977 - the HF/HCl column ratio, *J. Atmos. Chem.*, *5*, 385-394, 1987a.

Zander, R., G. Roland, L. Delbouille, A. Sauval, C. B. Farmer, and R. H. Norton, Column abundance and the long-term trend of hydrogen chloride (HCl) above the Jungfraujoch Station, *J. Atmos. Chem.*, *5*, 395-404, 1987b.

Zander, R., M. R. Gunson, J. C. Foster, C. P. Rinsland, and J. Namkung, Stratospheric $ClONO_2$, HCl, and HF concentration profiles derived from Atmospheric Trace Molecule Spectroscopy Experiment Spacelab 3 observations: an update, *J. Geophys. Res.*, *95*, 20,519-20,525, 1990.

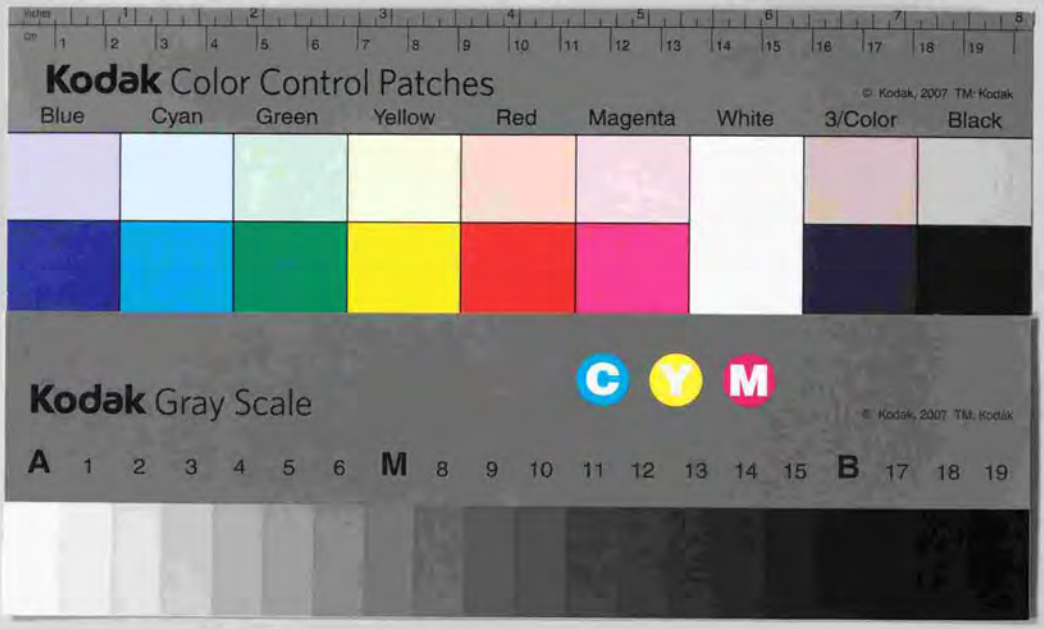
Kodak Color Control Patches
© Kodak, 2007 TM: Kodak
Blue
Cyan
Green
Yellow
Red
Magenta
White
3/Color
Black
Kodak Gray Scale
C
Y
M
© Kodak, 2007 TM: Kodak
A 1 2 3 4 5 6 M 8 9 10 11 12 13 14 15 B 17 18 19